Identification of Breathing Cracks in a Beam Structure with Entropy

by

S.R. Buddhi Wimarshana

A thesis submitted to
the Faculty of Graduate Studies of
The University of Manitoba
in partial fulfilment of
the requirements for the degree of
MASTER OF SCIENCE

Department of Mechanical Engineering
Faculty of Engineering
University of Manitoba
Winnipeg, Manitoba

Abstract

During vibration of engineering structures, fatigue cracks may exhibit repetitive crack open-close breathing like phenomenon which ultimately result in a distinct crack type, breathing cracks. This breathing phenomenon generates bi-linearity and irregularities in vibration signals of the cracked structure which carry useful information about the crack occurrence. In this thesis, the concept of entropy is employed to quantify this bi-linearity/irregularity of the vibration response so as to evaluate crack severity. To increase the sensitivity of the entropy calculation to detect the damage severity, sample entropy and quantized approximation of sample entropy are merged with wavelet transformation (WT) which is capable of amplifying the weak irregularities in vibration signal caused by small and initial breathing cracks. A cantilever beam with a breathing crack is studied to asses proposed crack identification method under two vibration conditions with sinusoidal and random excitations. An iterative numerical model is established to generate accurate time domain vibration responses of the cantilever with a breathing crack. Through both numerical simulations and experimental testing, the breathing crack identification with entropy under sinusoidal excitation is studied first and proven to be effective. Then, the crack identification sensitivity under lower excitation frequencies is further improved by parametric optimization of sample entropy and WT. Finally, effective breathing crack identification under general random excitations are experimentally studied and realized using frequency response functions (FRFs) which adapts the proposed crack identification technique to the incurred extra complexity due to random nature of the excitation and structural response.

Acknowledgments

I would first like to give a big thank to my thesis supervisor Dr. Nan Wu and my co-supervisor Dr. Christine Wu for their tremendous support, guidance, valuable ideas and their encouragements which served immensely preparing this thesis. They always kept their doors open to me whenever I ran into a trouble spot or had a question about my research or in any academic writings. I was given plenty of freedom to stretch my imagination to come up with new ideas, and they steered me to right direction whenever they thought it was necessary.

This thesis would have never been possible without these four most important people in my life. My mother and father (Padmalatha and Wimalajeewa), my little sister (Kaushalya) and who kept me always motivated and strong, my partner Samali Ruwandika. I am grateful to them wholeheartedly.

My sincere thanks to all of you,

S.R. Buddhi Wimarshana.

Contents

List of Tables

List of Figures

Nomenclature

a	scaling parameter of wavelet transformation
a(ω)	acceleration in frequency domain
b	width of the cantilever beam/ shift parameter in wavelet transformation
d	damaged beam/ damped vibration
E	Young's modulus
f(ω)	force excitation in frequency domain
F(t)	force excitation in time domain
h	thickness of the cantilever beam/ healthy beam
h_c	crack depth
H(ω)	frequency response function
k	positive constant in sample entropy measure
L	beam span of the cantilever beam
L_c	distance to the breathing crack from the fixed end of the cantilever beam
m	embedding dimension of entropy measures
n	vibration mode number
N	number of data points in a signal
q	general coordinate in mode superposition equation
Q	generalized force
r	parameter of entropy describing the maximum distance between two vectors which are considered to match

$R_{ff}(\tau)$	auto correlation function of force excitation in time lag of τ
$R_{af}(\tau)$	cross correlation function of acceleration and force in time lag of τ
$S_{ff}(\omega)$	auto spectral density of auto correlation function of force
$S_{af}(\omega)$	cross spectral density of cross correlation function of acceleration and force
t	time
w	lateral deflection of a beam
x	distance in beam span direction from fixed end of the cantilever beam
ζ	damping ratio
ρ	density
τ	time variable in Duhamel integration/ time lag
ω	excitation frequency in rad/s

AVG	Average
DFT	Discrete Fourier Transform
FRF	Frequency Response Function
QASE	Quantized Approximation of Sample Entropy
RSS	Root Sum Square
SampEn	Sample Entropy
SD	Standard Deviation
SNR	Signal-to-Noise Ratio
WT	Wavelet Transformation

List of Appendices

Chapter 1

Introduction

Identification of structural damages, which refers to detection and evaluation of these damages such as cracks, notches and delaminations, especially at their earliest stage is a vital process in engineering to avoid calamitous and irreparable damages. Closed fatigue cracks are a more evident damage type exhibited by many engineering structures. Crack breathing (repetitive opening and closing) is a common phenomenon and it is noted during the dynamic deformation of engineering structures with closed fatigue cracks. Identification of these cracks at their earliest stage is of utmost importance, but the bi-linear dynamic behavior of the structures with breathing cracks makes them difficult to be detected by traditional damage detection techniques and analytically more rigorous compared to their counterpart; the open cracks [1]. The recent studies have started to exploit the complex dynamic behavior of the breathing cracks envisioning better damage identification techniques [2]. In this context, entropy measures are a valuable tool for the quantification of complexity of dynamic systems [3]; therefore, entropy can be employed as a tool to develop a high sensitivity breathing crack identification technique.

During the lifespan of an engineering structure, it can be susceptible to fatigue cracks due to various cyclic-fluctuating loadings acting on the structure. These fatigue cracks, do not remain always open during dynamic loading conditions. The collective effect of static deflection of the

structure due to its self-weight and dead loads, and dynamic deflection due to vibration effect, can cause the crack to remain open at all times, or open and close regularly, or remain completely close. If the crack remains open all the times during vibration, then it is considered as an open crack. In the situations where the vibration amplitudes are larger compared to the static deflection of the structure, then the crack will open and close alternatively exhibiting a breathing-like behavior [4]. The cracks showing this behavior are generally called breathing cracks and unlike the open cracks, these breathing cracks introduce bi-linear dynamic behavior to the system [5]. This bi-linear dynamic behavior raises three major challenges in studies related to breathing crack identification. The first challenge faced by the researchers is, theoretical modeling (or mathematical modeling) of breathing cracks is much more complex than the modeling of simpler open cracks [4], but development of such complex theoretical models are essential for more accurate damage detection techniques [6]. The second difficulty arises when these breathing cracks are studied experimentally. It is more difficult to initiate and propagate an appropriate breathing crack experimentally, which is one possible reason for the few experimental studies found in literature dealing with realistic breathing cracks [7]. The next challenge is, the changes in the dynamic characteristics of the structure due to a breathing crack are smaller compared to the changes caused by an open crack with the same size, which leads to more difficulties in detecting these breathing cracks [5]. Even though the breathing effect of cracks in the presence of vibration of structures had been recognized since 1940s [8], viable solutions for the aforementioned challenges are not yet fully revealed.

During the past few decades, numerous methods have been proposed in breathing crack identification related studies. In the literature, two distinct numerical modeling approaches are found facilitating this purpose. The first approach, open crack models, are the simplest modeling

technique among the two, but as the name implies, these models assume that the crack is open always, hence they avoid the complexity incurred by the bi-linear dynamic nature from crack opening and closing. On the other hand, it is necessary to exploit the true bi-linear nature of the crack for developing accurate [4] and early-detection [9] of these breathing cracks. Hence, the second approach of numerical modeling, breathing crack models, is developed solely to serve these purposes by considering the bi-linearity.

In this thesis, a breathing crack numerical modeling technique is employed to fully exploit the bi-linear dynamic characteristics of the breathing cracks to develop an early detection and efficient evaluation technique of breathing cracks. A mathematical modeling technique combined with an iterative process developed by Wu [10] is employed to numerically interpret breathing crack dynamics, and the method is further improved by incorporating an important vibration aspect, damping effect. The developed model uses fracture mechanics theorem in conjunction with iterative numerical scheme to accurately generate the bi-linear vibration response of a beam structure having a breathing crack.

Furthermore, these breathing cracks generate irregularities in the vibration response of the structure. Entropy is a measure which can quantify these irregularities; therefore, in this thesis entropy is used as the central tool in developing the breathing crack identification technique. The idea of entropy was initially developed by Shannon [11] to quantify the amount of information in a communication signal. Then the idea was evolved to dynamical systems to quantify the system complexity, and today several entropy measures have been derived from the original idea and found useful in various applications [3]. In this thesis, sample entropy (SampEn) is employed as the main entropy tool to develop the high sensitivity breathing crack identification methodology;

this is primarily due to its capability in accurate quantification of irregularities with short and noisy data. In addition, to achieve smaller computational times in crack identification process, a derivation of sample entropy, quantized approximation of sample entropy (QASE) is used. Further, these two entropy measures are used in conjunction with two other signal processing tools, accordingly, to enhance the effectiveness of the proposed breathing crack identification technique.

In this thesis, wavelet transformation (WT) and frequency response function (FRF) are used as breathing crack identification aiding tools collectively with the main concept of entropy measures. Wavelet transformation is capable of magnifying irregularities in temporal or spatial signals [12,13]. Therefore, WT is a valuable tool to discern or amplify the weak irregularities in the time domain vibration signals, which are due to the breathing phenomenon of the repetitively opening and closing crack. Then, these processed (using WT) time domain vibration signals of the structure are quantified for the irregularities using the entropy measures so as to develop an effective breathing crack identification method. In addition, a dedicated study is conducted on how entropy and WT can be optimized to obtain the best crack identification results by using the proposed technique. Furthermore, in this thesis, breathing crack identification under random vibration, perhaps the most complex type of vibration type to handle and in fact the least studied in the literature, is also considered using the FRFs as an add-in tool. The FRF is capable of extracting the dynamic characteristics from a structure, and most importantly, the FRFs are independent of the excitation [14]. Therefore, FRF is coupled with the proposed breathing crack detection methodology to extend its capabilities to tackle the most common in nature, but conceptually more complex and rigorous, vibration conditions experienced by engineering structures under random excitations.

A cantilever beam with a breathing crack near the fixed end is selected as an applied case study to demonstrate the efficiency of breathing crack identification capabilities of the proposed technique using entropy with WT and FRF as add-in tools. This cantilever beam with a breathing crack represents a challenging case study, as it is studied under two types of vibration excitations, which are sinusoidal and random excitations. Sinusoidal excitation can have any excitation frequency, and hence capable of exciting different vibration modes of the structure, which ultimately affects the crack identification accuracy [2]. Contrary to (simpler) sinusoidal excitations, random excitations present higher complexity due to their inherent dynamic complexities. In this thesis, experimental studies are conducted in parallel to numerical simulations so as to validate the numerical results obtained for breathing crack identification.

Experimental results to assess the breathing crack identification results based on the numerically generated vibration response of the selected cantilever beam case study are obtained using an in-house laboratory test setup. Cantilever beams similar to the numerical studies are established, and several beams are constructed in order to achieve different crack depths. The location of the crack in all the beams are fixed near the clamped end of the cantilever beams, as it is in the numerical study. Then the experimental setup is used to obtain the dynamic responses of the beam under both sinusoidal and random excitations for breathing crack identification. Finally, the crack identification capabilities of the proposed technique is assessed through simulation and experimental studies to demonstrate the potential of the proposed method as a high sensitivity breathing crack identification technique for practical application.

1.1 Organization of the thesis

The organization of this thesis is such that, it is primarily based on three research papers which were prepared during the study of the presented work in this thesis (the three research papers are given in Appendix E). The thesis is divided in to seven chapters: introduction, literature review, methodology, followed by three chapters covering the findings presented in the three research papers, and a final chapter covering the conclusions and future works.

The literature review covers the research milestones that it passed in the last few decades when general damage identification techniques evolved in to modern vibration-based breathing crack identification methodologies. This particular chapter elaborates the relevant past studies, their contributions, their advantages which helped the progress in breathing crack identification, and at the end of the chapter, the problems which are still prevailing in those studies are revealed to set the objectives of the current study presented in this thesis. In the methodology chapter, it covers all the mathematical tools that are used in the proposed breathing crack identification technique.

After that, the chapters 4, 5 and 6 are dedicated to present the findings of the current study. They, as individual chapters, are originated from the three research papers that mentioned earlier. These three chapters provide detailed study of the proposed breathing crack identification technique. Chapter 4 presents breathing crack identification capabilities of the proposed crack identification technique under sinusoidal excitations. The second chapter provides further improvements to the proposed crack identification technique and the last chapter covers findings pertaining to breathing crack identification under general random excitations.

In the final chapter of conclusions and future works, the main findings of the thesis are concluded and some suggestions are given so as to further improve the proposed breathing crack identification technique envisioning a real world breathing crack identification methodology.

Chapter 2

Literature Survey

The effect of breathing cracks under vibration responses of the cracked engineering structures had been recognized since 1940s [4]. Since then, a number of major development steps in breathing crack identification have been introduced. In this chapter, evolvement of breathing crack identification techniques from general damage identification schemes to advanced vibration-based breathing crack identification techniques are elaborated. The deployment of entropy measures in damage detection, and how WT and FRF have influenced the damage identification methodologies in the past few decades are covered to give an insight to their advancement and, the areas where the technical gaps are found and where new thoughts can be implemented are covered in the final concluding section of this chapter, which draws the objectives of the thesis.

Structural health monitoring (SHM) with different damage identification techniques have been a largely concerned field of study for numerous researches from both industrial and academic communities. Local damage detection methods which are mostly referred to as non-destructive tests (NDTs), such as X-ray test, ultrasonic, and magnetic particle test etc., have been proven to be unsuitable in particular cases due to long inspection times [5], expensiveness of some methods, inability to reach the damaged area and most importantly they are not capable of

on-line real-time continuous detection of damages [5]. As a result, new research frontiers in SHM have turned towards global vibration-based structural damage detection methodologies, due to their on-line real-time continuous damage detection capabilities, ability of monitoring literally any structural part of interest and their cost effectiveness during long runs.

Vibration signals of a structure carries great amount of information about the healthiness of that particular structure. All vibration-based structural damage detection methods strive to extract these damage related vibration information effectively and efficiently and to interpret the damage which causing them. Numerous reviews [15–18] can be found in the literature on vibration based damage detection methodologies proposed in the past several decades. Although many vibration based structural damage detection techniques and methodologies have been proposed, their development can mainly be divided into two: traditional and modern types [19]. The traditional type refers to damage detection solely depending on the direct changes in the modal parameters of the structure; such as modal frequencies [1,20,21], modal shapes [22,23], and frequency response functions [24,25]. These methods generally require experimental measures, which require multifarious instruments or manual operation, therefore traditional type of techniques are not convenient for online damage detection [19]. In addition, prime issues conflict them with today's engineering needs are, they have shown lesser sensitivity to initial stages of the damages and possess more dependence on the properties of the individual structures limiting them in expanding to universal methodologies. On the other hand, modern types depend on the online measured responses of the structure and use signal processing techniques and intelligent damage identification agents such as artificial neural networks (ANNs) [26–28] and genetic algorithms (GAs) for damage identification [29,30]. In addition to those intelligent damage identification agents, wavelet analysis is a signal processing technique [31], which gained popularity during

the last two decades as a structural damage detection tool using both spatial and temporal signals [12,32]. Then, the advantages of these modern type techniques are: higher sensitivity to initial damage stages, online measurements avoid operational halts of the system and have higher flexibility in expanding these techniques as universal methodologies. In this thesis, a modern vibration-based high sensitivity on-line damage detection methodology is proposed to utilize the full potential of the modern techniques, in a dedicated damage identification area, which is breathing crack identification.

Fatigue cracks are evident as breathing cracks in many occasions of structural damages. During vibration of the structure with sufficient amount of deflection of the structure around the crack, the crack undergoes opening and closing repetitively which is generally termed as breathing phenomenon. In the literature, many crack modeling techniques have been proposed by various studies to find viable vibration based methods for breathing crack identification. Broadly, all these crack models fall into two categories: open crack models and breathing crack models [1]. In open crack models, the crack is considered remain open during the vibration and it is the most widely used [33,34] modeling technique to avoid the complexity resulting from bi-linearity of the breathing crack models. These models are less sensitive to smaller crack depths [35–38] and lead to lesser crack severity predictions than what they really are [4]. Therefore, recent studies are more in the favor of breathing models, which mitigates those problems by mimicking the real open-close phenomenon of breathing cracks [1,39,40]. In a recent study, a mathematical modeling technique combined with an iterative process has been developed by Wu [10] and the method claims generating accurate reproduction of bi-linear dynamic properties of the breathing fatigue cracks computationally. The same modeling technique is used in this thesis, with further

improvements by including damping to generate more accurate and realistic time series vibrational signals of a beam with breathing crack.

Breathing crack models are the only way for developing more sensitive breathing crack detection techniques which are capable of identifying smaller initial crack depths. But even these crack modeling techniques still have not been able to reach effective high sensitivity breathing crack identification. This is due to the fact that, while development of accurate breathing crack modeling techniques are important for overall accurate crack detection, the analytical methodologies employed in analyzing the dynamic signals of a breathing crack mathematical model or a breathing cracked structure play a vital role in reaching higher sensitivities in identification of smaller initial breathing cracks. This is because of the weak signature of any distinguishable dynamic irregularities generated by smaller crack severities compared to moderate or larger crack depths; without effective analytical methods, these dynamic irregularities are undetectable. Cheng *et al.* have employed a breathing crack model to study a beam structure with a breathing crack [1], but the study has been limited to moderate sized cracks (around 30% crack depth with respect to the total thickness of the beam) due to direct analysis of time and frequency domain information. This lower crack identification capabilities are seen in other proposed techniques [4] those belong to the breathing crack identification era of direct analytical methods are the way of analysis. Several years later, Douka and Hadjileontiadis have derived instantaneous frequencies using a breathing crack model generated dynamic signals [6] by which the method deviates from direct analysis methods. Their numerical simulations show around 30% of crack depth identification (the percentage crack depth ratio with respect to the thickness of the beam) only with periodic excitations of the structure. Nguyen and Olatunbosun have employed wavelet transformation on strain-time history generated by a

breathing crack model. But the model is capable of identifying cracks larger than 19% of crack depth. In a recent study, Gianni *et al*. have conducted a numerical study on a harmonically excited cantilever beam using a breathing crack model and then a multi modal analysis is applied to realize the breathing crack identification [9]. Their numerical results claim ability in identifying cracks larger than 5%. But the method is based on a less-viable condition in reality that is, the structure is required to be excited near one of its modal frequencies. In this thesis, the concept of entropy is employed to develop a high sensitivity breathing crack identification technique which does not depend on special dynamic conditions which are hard to be realized in real world application stages.

Entropy is a measure, which can quantify the irregularity in dynamic signals, and numerous entropy measures have been introduced since its introduction into dynamic systems by Kolmogorov and Sinai [41–43]. Higher the irregularity of a dynamic response of a given system, higher the entropy values are. Evaluation of complexity values of time-series data based on entropy measures are well studied in different disciplines including biomedical studies [44,45], in characterizing human motion [46], image processing [47,48], in financial market studies [49] and so on. In the damage detection perspective, in the recent studies, various entropy measures are being applied in rotary machines to diagnose various damages. Yan and Gao [50] have employed approximate entropy (ApEn) as a diagnosis tool to identify the different deterioration phases under several damage modes of rolling-element bearings. The authors claim more than 200% increment in ApEn values even under light damages to the bearings. Zhang *et al*. [51] have introduced multi-scale entropy (MSE) measures for the first time in fault diagnosis. The mentioned work has been able to produce better results with MSE over single scale-based

entropy measures. Similar bearing fault diagnosis has been done using permutation entropy (PE) [52] and multiscale permutation entropy (MPE) [53] with improved accuracies.

From the literature survey, only few research works have been carried out on structural damage detection using entropy as a tool. Yang et al. [54] have employed entropy measures in detecting cracks in beam-like structures. The crack they considered is limited only to open cracks, and direct employment of entropy limited their approaches effective only for larger cracks. The entropy itself alone is found to be not quite sensitive for the crack detection. This is due to the weak signature of the irregularities from the breathing. In this context, WT is a valuable add-in tool which can be used in conjunction with the entropy measures. The advantage of WT is the ability to perform local analysis of a signal by zooming on any desired segment of the temporal or special signal [55]. This key feature of WT has been merged with the entropy concept to reveal information concealed in signals. This idea is popular in biomedical studies such as to analyze brain signals [56]. But, in the field of structural damage detection, only few studies have been done so far. Browne *et al*. have studied feature extraction from sewer pipes for crack detection [57]. Ren and Sun [55] introduced the wavelet-entropy technique to notch detection in structures. Their study is limited to analysis of the sudden change in the vibration signal to find the occurrence of the damage, and the method lacks in damage severity estimation during its operation with an existing damage.

The ultimate goal of all these crack identification methods is, perhaps to be implemented as real-world crack identification methodologies. But, in the event of that, the fundamental problem faced by most of these crack detection methods is, the distinct vibration patterns observed by the structures in real world conditions by which drastically diminish the claimed crack identification

capabilities of the proposed methods. This is due to the fact that, these methods are not capable of tackling random vibrations, which is the most evident vibration pattern experienced by most of the structures. When it comes to handle random vibration signals, frequency response function (FRF) is a very useful tool. The key fact about FRFs is, the FRFs are capable of extracting the dynamic characteristics from a structure and most importantly, the FRFs are independent of the excitation type of the structure [14]. Traditionally, FRFs have been used to identify breathing cracks using super harmonics (or modulation lobes) of the excitation [1] which are less effective in the presence of noise in analyzed signals. More effective use of FRFs can be seen with methods using derivatives of FRFs. Owolabi *et al*. have employed normalized FRF amplitudes to locate and identify the crack depths of open cracks [24]. Luzzato has employed two distinct damage rates, which are derived from FRFs, to effectively identify the geometrical crack rates [58]. But this study is based on the damage rates, and the damage rates that he has simulated, as claimed by himself, have a weak probability of occurrence in the real world applications. In this thesis, FRFs are used as an add-in tool with main entropy tool to aid in breathing crack identification under random excitation of the structures.

2.1 Research objectives

The performed literature survey reveals that the previous crack identification techniques are lack in early detection of the breathing cracks due to their lower crack identification sensitivities to initial small crack depths. On the other hand, even though entropy is a better damage identification tool, it has never been employed in breathing crack identification, which is an area that can benefit from the core idea behind the entropy concept. In this thesis, the following objectives are set to achieve new steps in the breathing crack identification studies.

1. Development of a high sensitivity breathing crack identification technique, by employing the combined idea of wavelet-entropy, for the first time in breathing crack identification.

2. Further improvement of practicality and sensitivity of the proposed crack identification technique by optimizing the entropy and wavelet transformation parameters.

3. Adaptation of the proposed crack identification technique to more realistic operating conditions under random excitations by using derivatives of FRF as an add-in tool effectively with the main proposed crack identification technique, for the first time in breathing crack identification to identify breathing cracks.

4. Validation of the proposed breathing crack identification methodology with experimental studies to evaluate the viability of the proposed methodology in realistic breathing crack identification.

These objectives are realized in the next chapters of the thesis, and the progress and achievements of these objectives are concluded in the final chapter including some suggestions on future works.

Chapter 3

Theoretical Background and Methodology

Breathing crack identification presents number of challenges due to inherent complex dynamic properties of the bi-linear behavior and the weak signature of the breathing effect for smaller crack depths. In this chapter, the theoretical background of the various tools used in the proposed breathing crack identification technique is presented. First, in Section 3.1, the applied case study used to elaborate the proposed crack identification method is introduced. Then in the following sections, the numerical iterative breathing crack model, two entropy measures of SampEn and QASE, WT and finally FRF are given.

3.1 The breathing crack cantilever beam model

To demonstrate the viability of the proposed methodology to identify breathing cracks in structures based on time domain vibration signals, a vibrating cantilever beam with a breathing crack (near the fixed end) is studied. A schematic diagram of the beam structure is shown in Figure 3.1.

The beam is considered as an ASTM A36 steel beam of a unit length (in meters). The cross section is $b \times h$, where b and h are the width and the thickness of the beam, respectively. The

distance to the breathing fatigue crack from the fixed end is L_c, and it should be noted that, in this thesis, the crack is considered to be on the top surface of the cuboid shaped slender beam. The depth of the crack or crack severity (h_c) is varied in the analysis from zero (healthy beam) to half of the beam thickness ($h/2$). The crack depth percentage is the percentage ratio of the crack depth, h_c, to total thickness, h, of the beam. Young's modulus of the beam is E and density is denoted by ρ. The beam is excited sinusoidally ($F(t)$) at its free end. The angular frequency of the excitation is ω and the time elapsed is denoted using t.

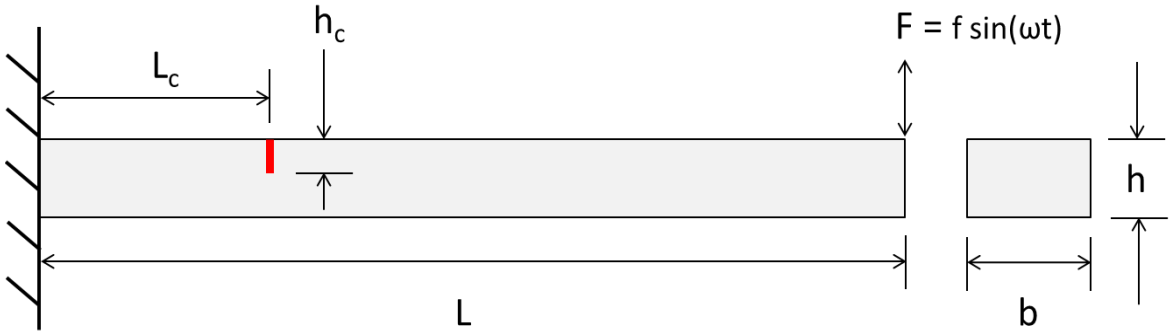

Figure 3. 1 - Cantilever beam with a breathing crack.

In the next section, one of the most important steps in developing a damage identification methodology is presented. That is formulating of a breathing crack model for accurate interpretation of the dynamic characteristics of the real breathing crack. The steps in mathematical formulation of the numerical iterative model for the mentioned cantilever beam with a breathing crack are presented in the following section.

3.2 Mathematical modeling of the cantilever beam with a breathing crack

As shown in Figure 3.1, a cantilever beam of length L and uniform cross section of $b \times h$ is considered. The breathing crack is located at L_c from the fixed end and the depth of the crack is h_c. According to the Euler-Bernoulli beam theory, the governing dynamic beam equation is:

$$EI\frac{\partial^4 w_{(x,t)}}{\partial x^4} + \rho A\frac{\partial^2 w_{(x,t)}}{\partial t^2} = F(x,t) \tag{3.1}$$

where I and A are the second moment of inertia of cross section and cross sectional area respectively. $w(x,t)$ is the vibration deflection of the beam at a distance x from the fixed end at time t and the dynamic loading applied at the beam tip is $F(x,t)$. The detailed derivation steps of the dynamic beam equation are given in Appendix A.

First, when the value of the slope on the left side of the crack is smaller than the one on the right side, the crack is in closed position, hence the beam can be treated as a healthy beam [10]. This is illustrated in the Figure 3.2. Figure 3.2 is an exaggerated view of the bending of the beam during vibration, and point 2 represents the crack position on the top surface of the beam and points 1 and 3 represent two points which are infinitesimally close to the crack point (the distance is marked as dx). The tangent values of angles α and θ represent the slopes of the beam sections to the left and to the right of the crack respectively. Both angles are measured in counterclockwise direction. Then, if $\tan\alpha \leq \tan\theta$, then the crack is in closed stage, the beam is treated as a healthy beam then.

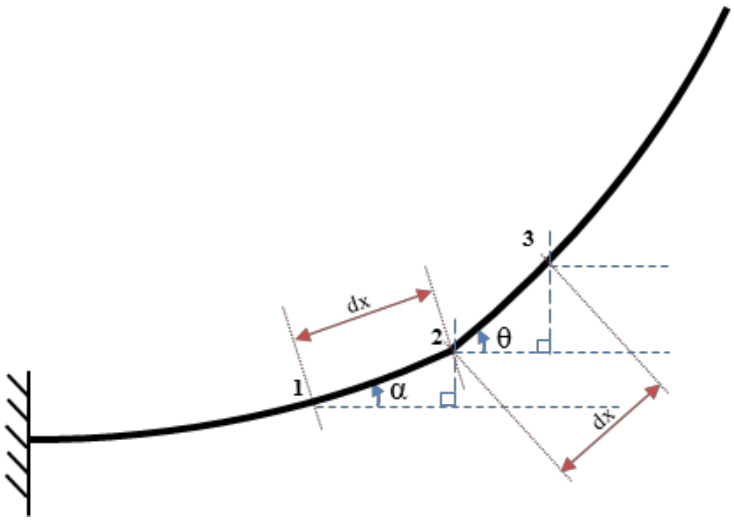

Figure 3. 2 - Slope discontinuity at the crack position of the cantilever beam during vibration.

Then using variable separable method the mode shapes of the beam with the closed crack can be found for n^{th} mode of vibration (the derivation is given in Appendix B):

$$0 \le x \le L: \qquad W_{n,h}(x) = A_1 \cos \beta_{n,h} x + A_2 \sin \beta_{n,h} x + A_3 \cosh \beta_{n,h} x + A_4 \sinh \beta_{n,h} x \qquad (3.2)$$

where A_1, A_2, A_3 and A_4 are unknown constants to be determined using boundary conditions and $\beta_{n,h}$ is given as:

$$\beta_{n,h}{}^4 = \frac{\rho A}{EI} \omega_{n,h}{}^2 \qquad (3.3)$$

and $\omega_{n,h}$ is the n^{th} mode modal (natural) frequency of the 'healthy' beam (closed crack). Applying the boundary conditions of the cantilever beam in equation (3.2) give us four linear

equations and we can solve them to find the n^{th} natural frequency of the beam, $\omega_{n,h}$, and the corresponding modal shape, $W_{n,h}(x)$, for the closed crack position.

Secondly, when the slope of the left side of the crack or larger than the right side, the crack is in open position and then the beam can be treated as an open crack beam or a damaged beam [10]. Now the beam is separated into two sections at the crack location to find its modal frequencies and the corresponding modal shapes. Let's assume that beam section to the left of the crack as section 1 and the section to the right as section 2. Then, the vibration mode shapes of the two beam sections with open crack are:

$$0 \le x \le L_c: \qquad W_{n,d1}(x) = A_5 \cos\beta_{n,d}x + A_6 \sin\beta_{n,d}x + A_7 \cosh\beta_{n,d}x + A_8 \sinh\beta_{n,d}x$$

$$L_c \le x \le L: \qquad W_{n,d2}(x) = A_9 \cos\beta_{n,d}x + A_{10} \sin\beta_{n,d}x + A_{11} \cosh\beta_{n,d}x + A_{12} \sinh\beta_{n,d}x \qquad (3.4)$$

and $\beta_{n,d}$ is given as:

$$\beta_{n,d}{}^4 = \frac{\rho A}{EI}\omega_{n,d}{}^2 \qquad (3.5)$$

where $\omega_{n,d}$ is the n^{th} mode modal frequency of the 'damaged' beam (open crack). The eight boundary conditions required to solve equation (4), are as follows:

$$x = 0: \qquad W_{d1}(x) = 0, \qquad \frac{dW_{d1}(x)}{dx} = 0;$$

$$x = L_c: \qquad W_{d1}(x) = W_{d2}(x), \qquad \frac{dW_{d1}(x)}{dx} + \Theta L\frac{d^2W_{d1}(x)}{dx^2} = \frac{dW_{d2}(x)}{dx},$$

$$\frac{d^2W_{d1}(x)}{dx^2} = \frac{d^2W_{d2}(x)}{dx^2}, \quad \frac{d^3W_{d1}(x)}{dx^3} = \frac{d^3W_{d2}(x)}{dx^3};$$

$$x = L: \qquad \frac{d^2 W_{d2}(x)}{dx^2} = 0, \qquad \frac{d^3 W_{d2}(x)}{dx^3} = 0 \tag{3.6}$$

The parameter Θ represents the additional non-dimensional flexibility of the beam due to the opening crack [10], which is defined as a function of the crack depth and calculated from fracture mechanics and Castigliano's theorem [59],

$$\Theta = 6\pi \frac{h}{L} \int_0^{h_c/h} x \left(\frac{0.923 + 0.199(1 - \sin(\frac{\pi}{2}x))^4}{\cos(\frac{\pi}{2}x)} \right)^2 \frac{\tan(\frac{\pi}{2}x)}{\frac{\pi}{2}x} dx \tag{3.7}$$

Substituting equation (3.4) into boundary conditions of the cantilever considering the crack opening given in equation (3.6), the n^{th} natural frequency of the beam, $\omega_{n,d}$, and the corresponding modal shape, $W_{n,d}(x)$,can be solved.

Then, the full vibration response of the beam can be found using the mode superposition:

$$w(x,t) = \sum_{n=1}^{\infty} W_n(x) q_n(t) \tag{3.8}$$

where n is the mode number and $q_n(t)$ is the generalized coordinate part. The process of obtaining full vibration response of the beam using the novel iterative method is described briefly in the following paragraphs.

As it was mentioned before, during the vibration beam undergoes two structural states, open crack (damaged beam) and closed crack (healthy beam) stages with different stiffness at the crack position. Due to this bi-linear behavior of the beam, vibrational characteristics of the beam keep changing. Hence, it is not easy to derive accurate analytical vibration solution of the beam

subjected to external excitations with variable stiffness of the structure [10]. Therefore, an iterative numerical approach is used to find the final vibration solution ($w(x,t)$) of the beam [10]. The full vibration responses of the closed crack and the open crack stages of the beam at the i^{th} time step (t_i), considering damping (ζ is damping ratio), at any position (x) on the beam with the judgment of the crack breathing states are given below:

If the slope on the left side of the crack is larger than the slope on the right side (i.e. the closed crack/ healthy stage), the deflection of the beam is given by:

$$w(x,t_i)=\sum_{n=1}^{\infty}W_{n,h}(x)q_{n,h}(t_i) \tag{3.9}$$

$$q_{n,h}(t_i)=e^{-\varsigma\omega_{n,h}(t_i-\tau)}(A_{n,h}\cos\omega_{n,h}t_i+B_{n,h}\sin\omega_{n,h}t_i)+$$

$$+\frac{1}{\rho A b'_{n,h}\omega^d_{n,h}}\int_{t_{i-1}}^{t_i}e^{-\varsigma\omega_{n,h}(t_i-\tau)}Q_{n,h}(\tau)\sin[\omega^d_{n,h}(t_i-\tau)]d\tau \tag{3.10}$$

where, damped natural frequency is given by, $\omega^d_{n,h}=\sqrt{1-\zeta^2}\omega_{n,h}$, $Q_{n,h}(\tau)$ is the generalized force function and given by, $Q_{n,h}(\tau)=\int_0^L F(x,t_i)W_{n,h}(x)dx$, $b'_{n,h}=\int_0^L W^2_{n,h}(x)\,dx$, and τ is a variable of time in Duhamel integration. In this iterative process, $A_{n,h}$ and $B_{n,h}$ are related to the vibration response from the previous iteration step.

$$B_{n,h}=\frac{e^{\varsigma\omega_{n,h}t_{i-1}}\cos\left(\omega^d_{n,h}\,t_{i-1}\right)\left(\frac{dq_n(t_{i-1})}{dt}+\varsigma\;\omega\;q_n(t_{i-1})\right)+q_n(t_{i-1})\;e^{\varsigma\omega_{n,h}t_{i-1}}\omega^d_{n,h}\;\sin\left(\omega^d_{n,h}t_{i-1}\right)}{\omega^d_{n,h}}$$

$$A_{n,h}=\frac{q_n(t_{i-1})\;e^{\varsigma\omega_{n,h}t_{i-1}}-B_{n,h}\sin\left(\omega^d_{n,h}t_{i-1}\right)}{\cos\left(\omega^d_{n,h}t_{i-1}\right)} \tag{3.11}$$

$q_n(t_{i-1})$ terms in equation (3.11) is related with either healthy or damaged beam responses depending on the vibration state of the beam at the previous iterative time step.

On the other hand, if slope on the left side of the crack is smaller than the slope on the right side (i.e. the open crack/damaged stage), similar set of equations can be written as:

$$w(x,t_i) = \sum_{n=1}^{\infty} W_{n,d}(x) q_{n,d}(t_i) \tag{3.12}$$

$$q_{n,d}(t_i) = e^{-\varsigma\omega_{n,d}(t_i-\tau)}(A_{n,d}\cos\omega_{n,d}t_i + B_{n,d}\sin\omega_{n,d}t_i) + \\ + \frac{1}{\rho A b'_{n,d}\omega^d_{n,d}} \int_{t_{i-1}}^{t_i} e^{-\varsigma\omega_{n,d}(t_i-\tau)} Q_{n,d}(\tau)\sin[\omega^d_{n,d}(t_i-\tau)]d\tau \tag{3.13}$$

where, $\omega^d_{n,d} = \sqrt{1-\zeta^2}\omega_{n,d}$, $Q_{n,d}(\tau) = \int_0^L F(x,t_i)W_{n,d}(x)dx$, $b'_{n,d} = \int_0^L W^2_{n,d}(x)\,dx$ and similar to the healthy beam stage stated before, $A_{n,d}$ and $B_{n,d}$ are related to the vibration response from previous iteration step.

$$B_{n,d} = \frac{e^{\varsigma\omega_{n,d}t_{i-1}}\cos\left(\omega^d_{n,d}\ t_{i-1}\right)\left(\frac{dq_n(t_{i-1})}{dt} + \varsigma\ \omega\ q_n(t_{i-1})\right) + q_n(t_{i-1})\ e^{\varsigma\omega_{n,d}t_{i-1}}\omega^d_{n,d}\ \sin\left(\omega^d_{n,d}t_{i-1}\right)}{\omega^d_{n,d}}$$

$$A_{n,d} = \frac{q_n(t_{i-1})\ e^{\varsigma\omega_{n,d}t_{i-1}} - B_{n,d}\sin\left(\omega^d_{n,d}t_{i-1}\right)}{\cos\left(\omega^d_{n,d}t_{i-1}\right)} \tag{3.14}$$

In equations (3.9) to (3.14), the subscripts of n denotes the n^{th} mode of the vibration, h and d denote the healthy and damaged vibration stages of the beam with closed and open crack, respectively. From the theoretical model described above, it is noticed that the beam structure with breathing crack keeps changing between the healthy and damaged stages repetitively with

different natural frequencies and mode shapes during its vibration. The change of the structure during the vibration introduces additional irregularity of the vibration signal compared with the intact structure.

The next section presents the core technique used in the breathing crack identification methodology proposed in this thesis, which is entropy. The following section presents the SampEn, which is the main entropy tool used, and then following that section, QASE which is a derivative of the SampEn is presented.

3.3 Sample entropy (SampEn)

Entropy can quantify the irregularity of time domain signals so as to detect and evaluate the breathing crack, which generates irregularities in the structural vibration signals. SampEn is capable in well handling of short, noisy data samples with trouble-free implementation [45]. Let's take a time series X having N number of data points such as: $\{x(1), x(2), \ldots, x(N)\}$, then its irregularity can be quantified as follows.

First, template vectors of length m ('m' is called embedding dimension) are defined, such as;

$$X(1) = \{x(1), x(2), ..., x(m)\}$$

$$X(2) = \{x(2), x(3), ..., x(m+1)\}$$

…

$$X(N-3+1) = \{x(N-m+1), x(N-m+2), ..., x(N)\} \quad (3.15)$$

Then the Chebyshev distance between all template vectors are calculated, and lets denote it by $d[X_m(i), X_m(j)]$ and $i \neq j$. Then we define a probabilistic parameter $B_i^m(r)$ as follows,

$$B_i^m(r) = \frac{\#\text{ of } j \text{ such that } \mathrm{d}[X_m(i), X_m(j)] \leq r}{N-m-1} \qquad (1 \leq j \leq N-m,\ j \neq i) \tag{3.16}$$

where r is a pre-determined tolerance value taken as:

$$r = k \times SD(X) \tag{3.17}$$

In equation (3.17), k is a constant ($k > 0$) and SD stands for the standard deviation. Then we sum-up all the probabilistic values,

$$B^m(r) = (N-m)^{-1} \sum_{i=1}^{N-m} B_i^m(r) \tag{3.18}$$

Similarly, for template vectors of length $m+1$

$$A_i^{m+1}(r) = \frac{\#\text{ of } j \text{ such that } \mathrm{d}[X_{m+1}(i), X_{m+1}(j)] \leq r}{N-m-1} \qquad (1 \leq j \leq N-m,\ j \neq i) \tag{3.19}$$

and similar to equation (3.18),

$$A^{m+1}(r) = (N-m)^{-1} \sum_{i=1}^{N-m} A_i^{m+1}(r) \tag{3.20}$$

SampEn is then defined as:

$$SampEn(m, r, N) = -\ln\left[\frac{A^{m+1}(r)}{B^m(r)}\right] \tag{3.21}$$

In this derivation, $B^m(r)$ is the probability that two sequences will match for m points, on the other hand, $A^{m+1}(r)$ is the probability of match for $m+1$ points. Therefore, the quantity $[A^{m+1}(r)/B^m(r)]$ is the conditional probability that two sequences within a tolerance r for m points remain within r of each other at the next point [45]. Higher the irregularity of the time series, then lower this value of conditional probability, hence we obtain a higher SampEn value. In Appendix C a detailed calculation of SampEn is presented for a numerical example, which will help to have a better understanding of the process.

3.4 Quantized approximation of sample entropy (QASE)

The main objective behind the development of this new entropy measure, QASE, is to have improved computational efficiency (lower computational times) while quantifying the irregularities meaningfully [60]. In-order to achieve this improved computational efficiency, the core of the entropy calculation algorithm is based on a method called 'relative coarse quantization of time series data'. This coarse quantization of data hugely lowers the computational times over other entropy methods, and this quantization process is described below.

Let's consider a time series X having N number of data points; $\{x(1), x(2), \ldots., x(N)\}$, then relative coarse quantization of the time series is performed using a strictly positive parameter r, which defines the size of the quantization bins [48]. Then the quantized time series is:

$$X_q = \left\lfloor \frac{X - \min(x)}{r} \right\rfloor \qquad r > 0 \tag{3.22}$$

where $min(X)$ is the minimum value of the time series and $\lfloor . \rfloor$ denotes the floor function and it rounds off the value inside the function (to the nearest whole number) towards the negative infinity.

Then these quantized data samples are grouped (called 'vector groups') using an embedding dimension 'm'($m \in \mathbb{N}_1$). This embedding dimension determines the length of the vector. Let's call these vector groups as $V_j \; where \; 1 \leq j \leq N - m + 1$.

The vector identifiers (φ_j) are defined on these vector groups in the next step. It is done in the following way,

$$\varphi_j = \sum_{i=1}^{m} V_j(i) \; \lambda^{i-1}, \text{ where } \{1 \leq j \leq N - m + 1\} \text{ and } \lambda = \max(X_q) \tag{3.23}$$

Then it is possible to define the number of occurrences of each identifier as:

$$Q(\varphi_j) = \#\{ j \mid 1 \leq j \leq N - m + 1, \; [X_q(j), X_q(j+1), ..., X_q(j+m-1)] \in \varphi_j \} \tag{3.24}$$

Now, depending on these numbers of presence of each vector identifier, it is possible to construct the QASE in the following way.

The probability values of $B^m(r)$ and $A^{m+1}(r)$ in equations (3.18) and (3.20) respectively for SampEn calculations are approximated using occurrences of vector identifiers $Q(\varphi_j)$, as $\hat{B}^m(2r)$ and $\hat{A}^{m+1}(2r)$ respectively.

$$\hat{B}^m(2r) = (N-m)^{-1} \sum_{\varphi_m} Q(\varphi_m) \frac{Q(\varphi_m) - 1}{N - m - 1} \tag{3.25}$$

$$\hat{A}^{m+1}(2r) = (N-m)^{-1} \sum_{\varphi_{m+1}} Q(\varphi_{m+1}) \frac{Q(\varphi_{m+1}) - 1}{N - m - 1} \tag{3.26}$$

Then QASE is derived as,

$$QASE(m,2r) = -\ln\left[\frac{\hat{A}^{m+1}(2r)}{\hat{B}^{m}(2r)}\right] \tag{3.27}$$

A detailed sample calculation of QASE is given in Appendix C using a numerical example. Now, this entropy based breathing crack identification technique requires some appropriate techniques to improve its crack identification capabilities and sensitivity. In this thesis, two such techniques, called add-in tools, are incorporated with entropy: they are WT and FRFs. In the next two sections these two mathematical concepts are covered.

3.5 Wavelet transformation (WT)

Wavelet transformation is a signal processing method, which can magnify the perturbations or irregularities in signals [55] and be used to further enhance/support the entropy measurement to quantify the signal perturbations with higher sensitivity. The wavelet is a smooth and quickly vanishing oscillating function. The WT maps a temporal signal, $f(t)$, into two-dimensional domain (the time-scale plane) and is denoted by $W_f(a,b)$ given by;

$$W_f(a,b) = \frac{1}{\sqrt{a}}\int_{-\infty}^{+\infty} f(t)\quad h^*\left(\frac{t-b}{a}\right)\quad dt = \int_{-\infty}^{+\infty} f(t)\quad h^*_{ab}(t)\quad dt \tag{3.28}$$

where $h(t)$ is called the mother wavelet and the subscript * denotes the complex conjugate of the function. The basis functions of the transform, called daughter wavelets, are given by:

$$h_{ab}(t) = \frac{1}{\sqrt{a}}h\left(\frac{t-b}{a}\right)dt \tag{3.29}$$

$h_{ab}(t)$ is a set of basis functions obtained from the mother wavelet $h(t)$ by compression or dilation using scaling parameter a and temporal translation using shift parameter b [61].

In the present study, we use the 'symlet2' as the mother wavelet function and WT is realized using the MatLab® software package.

3.6 Frequency response function (FRF) – derivation for random vibration signals

There are many vibration analysis and testing tools available and FRF is one of them which is widely used to reveal dynamic characteristics of systems. FRF is a transfer function, expressed in the frequency domain as the name implies. The most important fact about using FRF for vibration analysis is, it is capable of characterizing the dynamics of the system independently from the type of excitation of the system [14].

Several forms of FRFs are available: such as receptance (or admittance), mobility, accelerance, etc. Receptance is the frequency domain ratio of displacement response of a structure to its force excitation. Mobility and accelerance share the same explanation but, the ratios are between velocity and force, and acceleration and force respectively. Due to readily available measurement techniques in accelerations, accelerance FRF is used in this thesis. Now, if the force input (excitation) to a system in the frequency domain is $f(\omega)$ and acceleration output (response) of the system is $a(\omega)$, then the accelerance FRF, $H(\omega)$ is defined by;

$$H(\omega) = \frac{a(\omega)}{f(\omega)} \tag{3.30}$$

where ω denotes the frequency domain.

In vibration analysis, the common practice is to compute the discrete Fourier transform (DFT) on the time domain signals acquired from experimental or analytical systems to obtain the frequency domain values. This requires both excitation and response to satisfy the Dirichlet condition, but random vibrations fail to satisfy this condition due to inherent properties of the random signals. This is solved using the correlation functions [14].

The autocorrelation function for the excitation $R_{ff}(\tau)$ is defined as the expected (E) or averaged value of the product of $(f(t).f(t+\tau))$ for a time lag of τ.

$$\mathrm{R_{ff}}(\tau) = \mathrm{E}\,[\mathrm{f(t).f(t+\tau)}] \tag{3.31}$$

Unlike the original excitation signal $f(t)$, this correlation function satisfies the Dirichlet condition, and thus the Fourier transformation can be obtained. The resulting parameter is called spectral density, in this case it is called auto spectral density, $\mathrm{S_{ff}}(\omega)$. The two sided auto spectral is defined as:

$$\mathrm{S_{ff}}(\omega) = \frac{1}{2\pi}\int_{-\infty}^{\infty} R_{ff}(\tau)\; e^{-i\omega\tau}\, d\tau \tag{3.32}$$

A similar concept is applied to the product of the two functions of excitation $f(t)$ and response $a(t)$ to produce cross correlation $\mathrm{R_{af}}(\tau)$ and cross spectral density $\mathrm{S_{af}}(\omega)$. Then, it is possible to calculate several FRF estimates using these auto- and cross spectral densities. The first estimate $\mathrm{H_1}(\omega)$ can be written as,

$$\mathrm{H}_1(\omega) = \frac{S_{af}}{S_{ff}} \tag{3.33}$$

and, the second estimate $\mathrm{H}_2(\omega)$ can be written as,

$$\mathrm{H}_2(\omega) = \frac{S_{aa}}{S_{fa}} \tag{3.34}$$

In this study, a third type of estimate is used, which is $\mathrm{H}_\mathrm{v}(\omega)$ and derived from auto- and cross spectra of the signals [62],

$$\mathrm{H}_\mathrm{v}(\omega) = \frac{\mathrm{S}_\mathrm{af}}{\left|\mathrm{S}_\mathrm{af}\right|} \times \sqrt{\frac{S_{aa}}{S_{ff}}} \tag{3.35}$$

and it is found during the analysis, this particular estimate gives better results compared to the other two estimates in crack identification process.

3.7 Summary

In this chapter, the applied case study (a cantilever beam with a breathing crack) to elaborate the proposed breathing crack identification method is presented. Then all the mathematical tools that are used in this thesis for deriving the crack identification technique; i.e. mathematical model of the breathing crack, entropy, WT and FRF, are explained to give a mathematical insight. Numerical iterative model is used to accurate re-production of the vibration signal of the breathing crack. The entropy is capable of quantifying the irregularities of the produced vibration signals, while WT is a feature magnification technique. The FRF is a tool that can be used to

extract dynamic characteristics of a system even under complex dynamic operating conditions of the structure.

In the next few chapters, these mathematical tools are appropriately used to collectively form the proposed breathing crack identification technique. In the next chapter, the applied case study is studied under sinusoidal excitation to find out the viability of the proposed crack identification method under these excitation conditions.

Chapter 4

Breathing Crack Identification under Sinusoidal Excitations

In this chapter, the proposed breathing crack identification methodology is revealed to show both how the mathematical tools explained in the previous chapter are combined to form the final breathing crack identification methodology, and the crack identification capabilities of the proposed methodology under sinusoidal excitations. Both numerical and experimental results presented and discussed to showcase the latter mentioned.

In Section 4.1, the overall crack identification methodology is discussed for the sinusoidally excited cantilever beam with a breathing crack. The in-house experimental setup for obtaining the experimental values for the analyzed case study is given in Section 4.2. Then the next section, Section 4.3, which covers the largest portion of this chapter, presents the results and discussions revealing both numerical and experimental results.

4.1 The overall process of crack identification using entropy with WT as an add-in tool

Breathing phenomenon of the fatigue cracks introduces the repetitive crack opening/closing and the change of the structure stiffness during the vibration leading to weak bi-linearity in the dynamic response of the beam. This imposes irregularities/perturbations in the vibration signals, which can be quantified by the entropies of these signals. It is actually a measure of crack severity since these irregularities are directly related to the depth of the crack. It is noted entropy itself is not sufficient enough to correlate the severity of the crack because of the weak signatures of the perturbations generated by the breathing cracks. However, once these weak perturbations are magnified using WT, those correlations can be easily found using the entropy measures of respective wavelet transformed vibration signals. This proposed breathing crack identification method is illustrated in Figure 4.1.

As it is shown in Figure 4.1, the first step of the derivation of the crack identification process is, building a mathematical model of the cantilever beam to obtain the vibration response of the tip of the beam considering the crack breathing with damping (refer Section 3.2). The accuracy of the dynamic response depends on the time step length used in the iterative process of the used mathematical model. Wu [10] claims the convergence of dynamic responses as long as the iterative time step is smaller 0.001 seconds. Therefore, a time step of 0.0001 seconds is used in the current study.

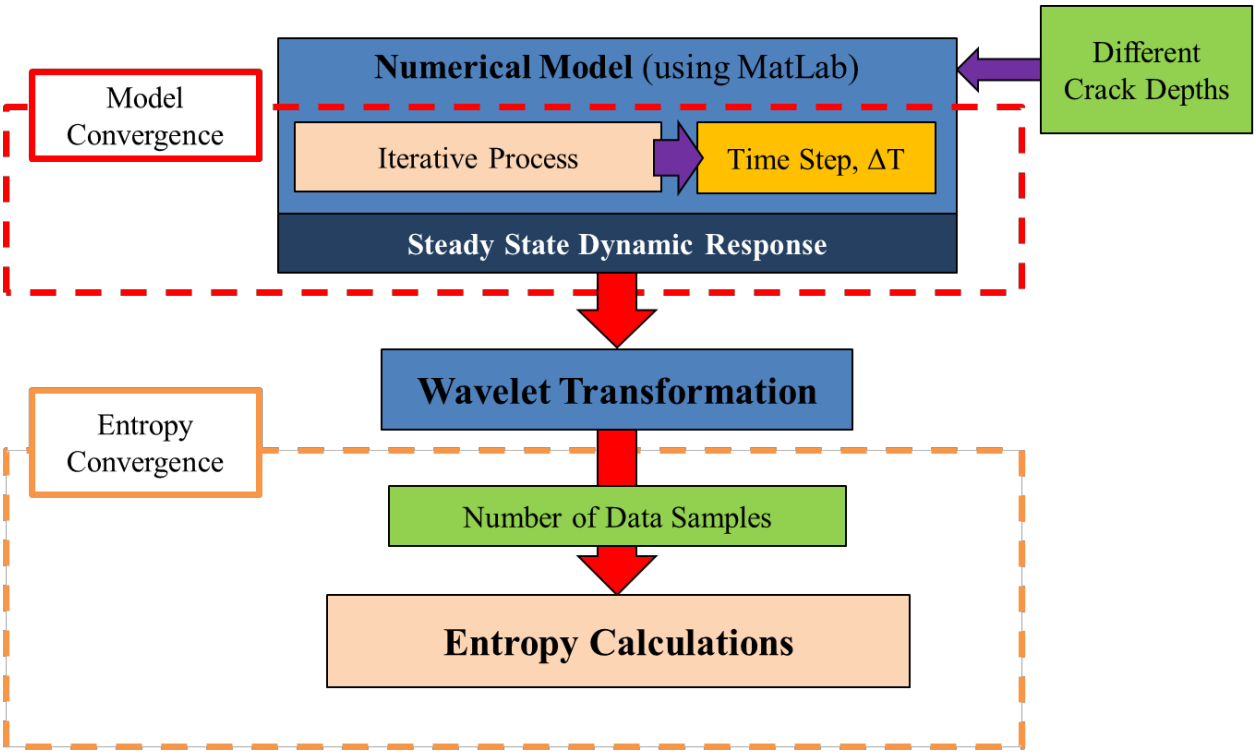

Figure 4. 1 - Flow chart of the overall crack identification process.

Then, by considering the damping effect during the vibration of the cantilever beam, the steady state response of the vibration signal is obtained and used for the entropy analysis. It should be noted that even though it is called ‘steady state’, it is not a pure steady state, rather a ‘semi-steady state’. The breathing phenomenon introduces extra axial force when the crack goes from open-to-close position during vibrating. In addition to that, the stiffness (equation (3.7)) around the crack varies between the open and closed crack stages of the vibrating beam (more details about these two stages are described in Section 3.2). Now due to these two reasons, perturbations appear in the vibration signal during the open-to-close and close-to-open stage transitions of the beam. Therefore it is never possible to have a pure steady state in the presence of a breathing crack. For the simplicity, this semi-steady state will be stated as ‘steady state’ throughout the paper.

The steady state vibration signal is then sent through WT, which magnifies the weak bi-linearity due to the breathing phenomenon of the crack. The transformed signal, WT coefficient, is then used in entropy calculations to quantify the irregularity of the vibration signal. Two entropy measures, SampEn and QASE, are used in this process individually for the quantification of the crack severity. The convergence of the entropy calculations with the number of sampled vibration signal is checked and convergence results can be found in Appendix D.

The same crack detection process is carried out repeatedly for the crack depths ranging from zero (i.e. healthy beam) to half of the thickness of the beam (50% crack depth percentage) in 1% of crack depth percentage intervals. The crack depth percentage is calculated as follows;

$$\text{Crack depth percentage} = \frac{\text{crack depth}}{\text{Thickness of the cantilever beam}} \times 100\% \tag{4.1}$$

Then, the percentage increment of the entropy values with respect to (w.r.t.) the healthy beam are calculated at each crack depth percentage in the following way;

$$\left.\begin{matrix}\text{Percentage increment of} \\ \text{Entropy w.r.t. Healthy Beam}\end{matrix}\right\} = \frac{\text{Entropy of the Cracked beam} - \text{Entropy of the Healthy beam}}{\text{Entropy of the Healthy beam}} \times 100\% \tag{4.2}$$

These percentage increments of entropies with respect to healthy beam at different crack depth percentages of the cantilever beam with a breathing crack are used to discuss the feasibility of the proposed breathing crack identification methodology under sinusoidal excitation.

Before proceeding to the results and discussion section, the following section provides the details about the in-house experimental setup for obtaining the experimental results of the case study; which are compared with the numerical results in the results and discussion section at the end of this chapter.

4.2 Experimental setup of the breathing crack cantilever beam under sinusoidal excitation

To validate the results and conclusions obtained through numerical simulations for the applied case study, measurements on relevant aluminum alloy (grade 6061-T6) cantilever beams are conducted. The breathing fatigue cracks are constructed by bonding three aluminum alloy beams together; the same technique has been used by Prime et al. [63] and Douka et al. [6] to demonstrate breathing cracks experimentally. Figure 4.2 illustrates the schematic diagram of the arrangement of the bonded beam pieces for constructing the beam with a 50% crack depth percentage.

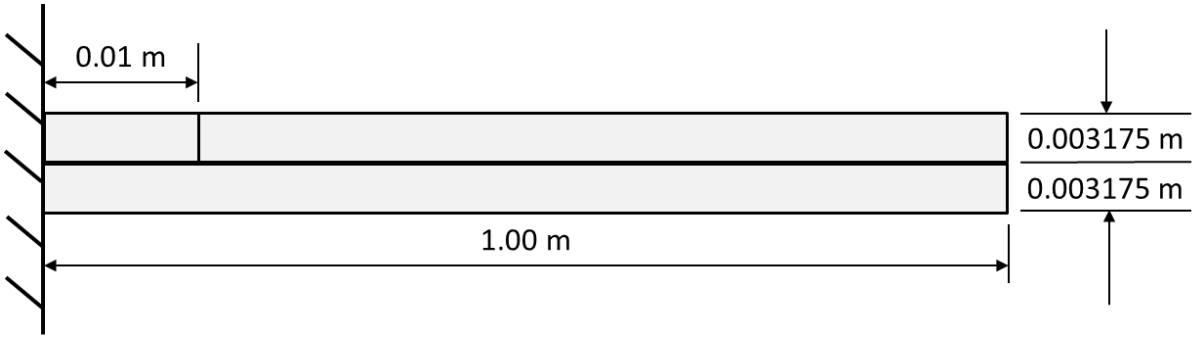

Figure 4. 2 - Schematic diagram of the constructed test beam for 50% crack depth percentage.

The crack is located 0.01 m from the fixed end of the cantilever beam, and the beam span is 1.00 m, these geometric parameters are same with the numerical model values which are presented in the next section. The healthy beam (0% crack depth percentage) is constructed by bonding two equivalent beams. This restricts the differences between healthy and cracked beams to the crack region [63]. Beams with 25% and 50% crack depth percentages are selected for the experimental validations due to ease of construction of those beams with the available materials.

The 25% crack depth percentage beam is constructed by bonding two aluminum alloy pieces of 0.0015875 m (1/16 inches) thickness on top of a continuous piece with 0.0047625 m (3/16 inches) thickness. The final thickness of all the constructed beams is 0.00635 m (1/4 inches) with 0.0254 m (1.00 inch) wide.

Figure 4.3 illustrates the experimental setup for obtaining the dynamic response from the 50% crack depth percentage beam. The beam is tightly clamped using four bolts to a steel clamping post which is solidly fixed to the concrete test bench (Figure 4.3.(b)). The free end of the beam is sinusoidally excited using a shaker (The Modal Shop – model 2100E11). PCB Piezotronics model 352A24 accelerometer weighing 0.8 g (sensitivity is 10.2 mV/(m/s^2) with $\pm$ 10% uncertainty) is located 0.10 m away from the free end of the beam (Figure 4.3.(c)). The sinusoidal signal generation and data acquisition are done using LMS SCADAS Mobile (type SCM05) data acquisition hardware and a personal computer which are integrated with the LMS Test.Lab software platform.

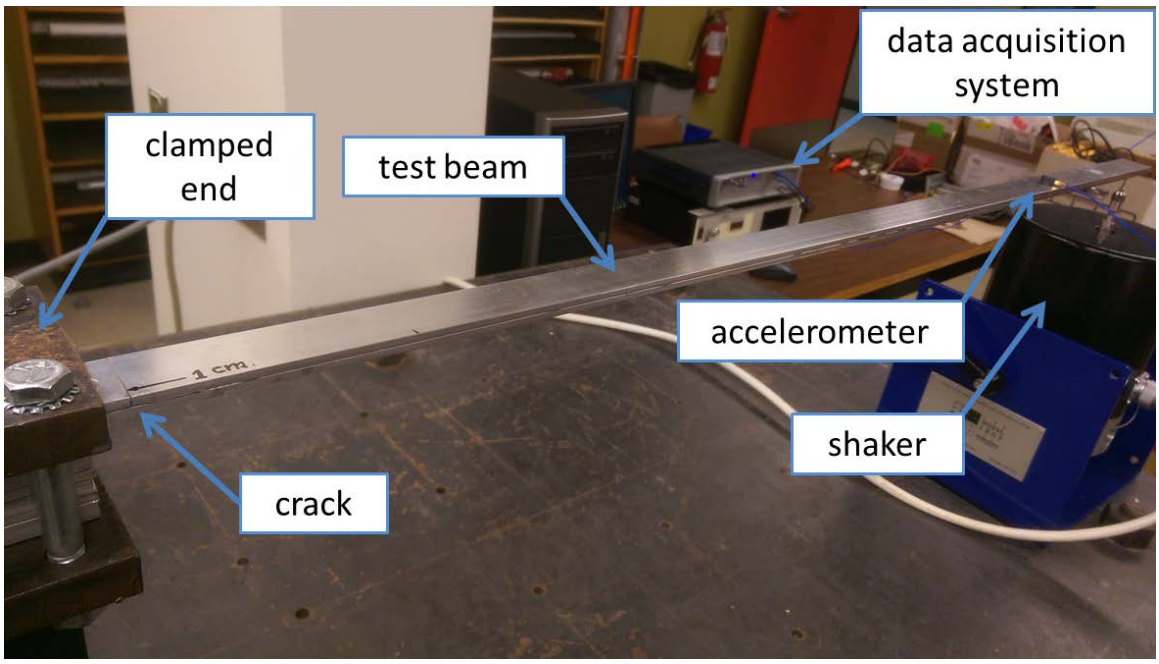

(a)

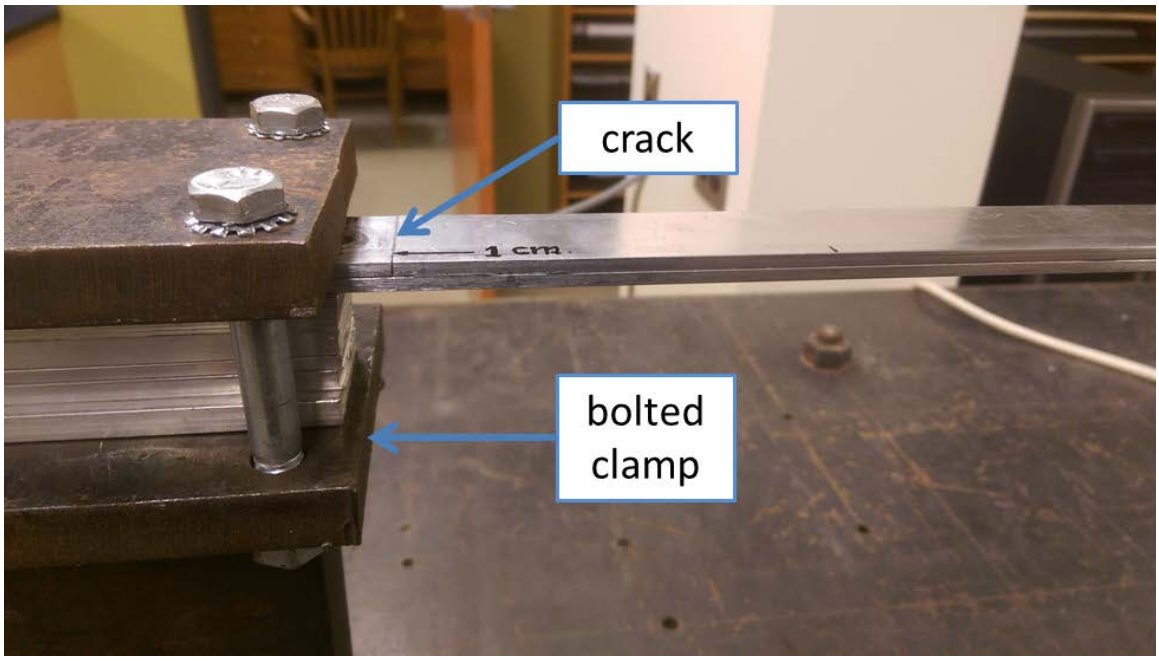

(b)

Figure 4. 3 - The experimental setup for obtaining dynamic responses of damaged and healthy aluminum alloy cantilever beams (a) the whole setup for testing of the beam with 50% crack depth percentage (b) the clamped end of the beam (c) the free end of the beam with shaker and the accelerometer (d) the data acquisition system (continued to the next page..).

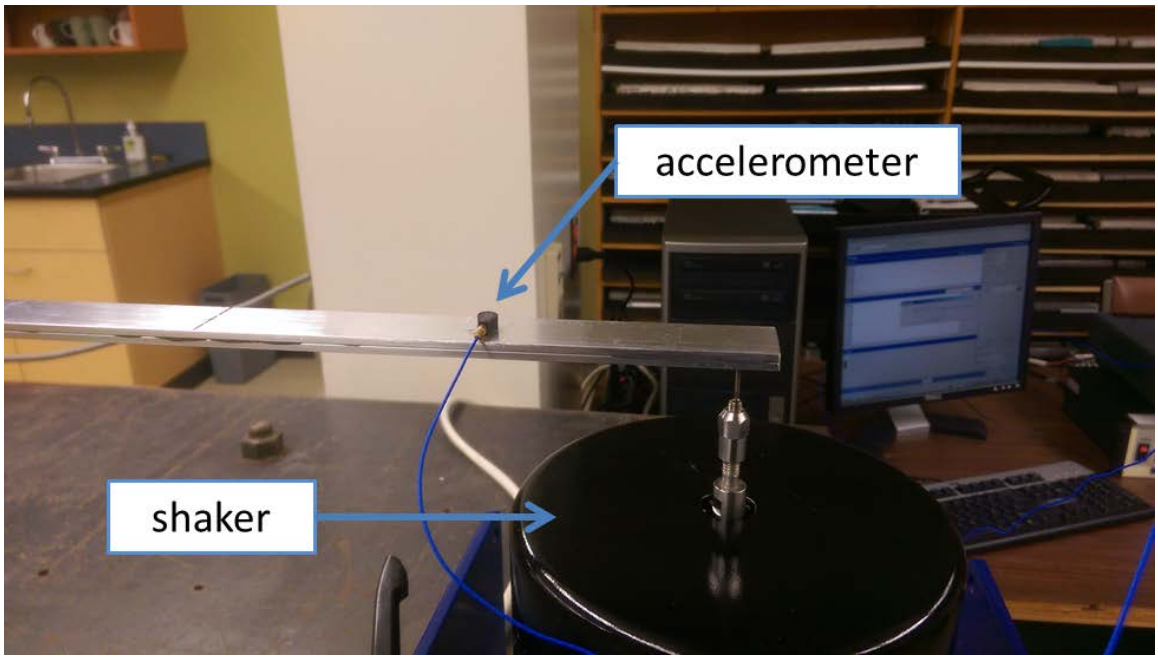

(c)

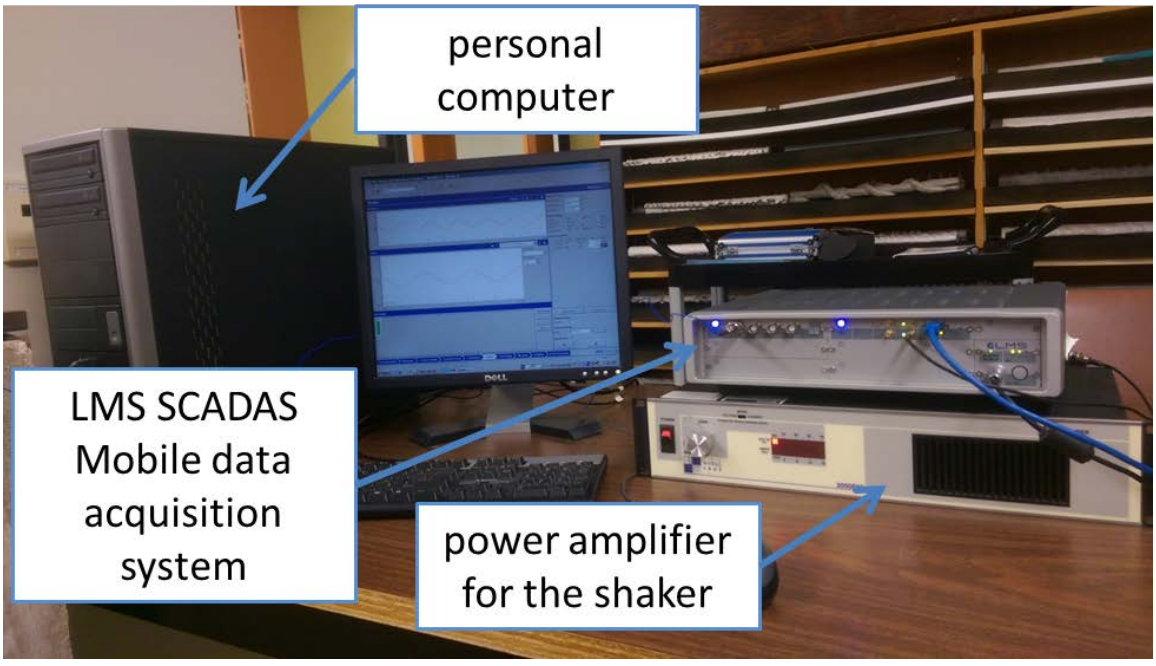

(d)

Figure 4. 4 - The experimental setup for obtaining dynamic responses of damaged and healthy aluminum alloy cantilever beams (a) the whole setup for testing of the beam with 50% crack depth percentage (b) the clamped end of the beam (c) the free end of the beam with shaker and the accelerometer (d) the data acquisition system.

The next section is dedicated for presenting the results and discussions related to the breathing crack identification under sinusoidal excitation of the applied case study. In this section, first the numerical results obtained using the numerical iterative breathing crack model (explained in Section 3.2) is presented. Then finally, the experimental results are compared with the numerical results.

4.3 Results and discussions

This section presents the results and corresponding discussions pertaining to the applied case study of the crack identification of the cantilever beam, which is described in Section 3.1. At first, the numerical simulation results are presented and discussed.

In Table 4.1, the dimensions, material properties of the beam and vibration parameters used in the numerical model are given.

Table 4. 1 - Dimensions and material properties of the cantilever beam.

Parameter	***Cantilever Beam***	***Crack***
L (m)	1	-
b (m)	0.05	-
h (m)	0.01	-
L_c (m)	-	0.01
h_c (m)	-	varies from 0.000 to 0.005 (in 0.0001 steps)
Young's modulus, E (GPa)	200	-
Density, ρ (kg/m3)	8000	-
Equivalent damping ratio for the first three modes, ζ	0.01	-
Magnitude of the sinusoidal excitation, f (N)	10	-

Table 4.2 provides the modal/natural frequencies of the beam at healthy and damaged beam stages (corresponding to closed crack and open crack stages) with different crack depth percentages obtained using the numerical simulations.

Table 4. 2 - Modal frequencies of the cantilever beam at Healthy and Damaged beam stages.

Vibration modes	***Modal frequencies (rad/s)*** *[difference from healthy beam stage]*					
	Healthy beam stage	Damaged beam stage, crack depth percentage (%)				
		10	20	30	40	50
1st Mode	50.7493	50.6449 [0.104]	50.3518 [0.397]	49.8451 [0.904]	49.0285 [1.721]	47.7010 [3.048]
2nd Mode	318.0405	317.4324 [0.608]	315.7480 [2.292]	312.9115 [5.129]	308.5311 [9.509]	301.8843 [16.156]
3rd Mode	890.5226	888.9328 [1.589]	884.5794 [5.943]	877.4149 [13.108]	866.7550 [23.767]	851.4848 [39.038]

During the simulation of the forced vibration response, the beam is subjected to sinusoidal excitation at the free end of the beam, $F(t) = f \sin(\omega t)$. The excitation frequency, ω, is within the first two modal frequencies of the beam (40 ~ 330 rad/s), and only the first three modes of vibrations are hence taken into consideration.

4.3.1 Dynamic responses of the breathing crack beam model

In this sub-section, several dynamic responses of the cantilever beam subjected to several selected excitation frequencies are presented with and without damping effect to reveal the accurate dynamic response re-production abilities of the iterative numerical breathing crack model. It is noted that more accurate vibration responses can be obtained with smaller iteration step length ($\Delta T = t_i - t_{i-1}$) as it is given in Section 4.1; and converged time step length of 0.0001s is used to generate the accurate vibration signals.

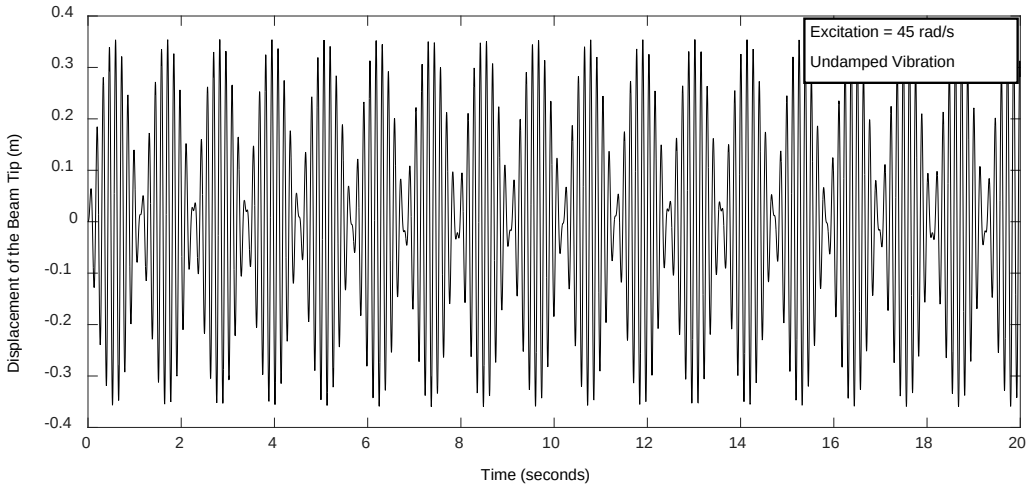

(a)

Figure 4. 5 - Dynamic responses at the free end of the cantilever beam, without damping under excitation frequencies of (a) 45 rad/s (b) 200 rad/s (c) 300 rad/s, and with the damping ratio of 0.01 under excitation frequencies of (d) 45 rad/s (e) 200 rad/s (f) 300 rad/s (continued to the next page..).

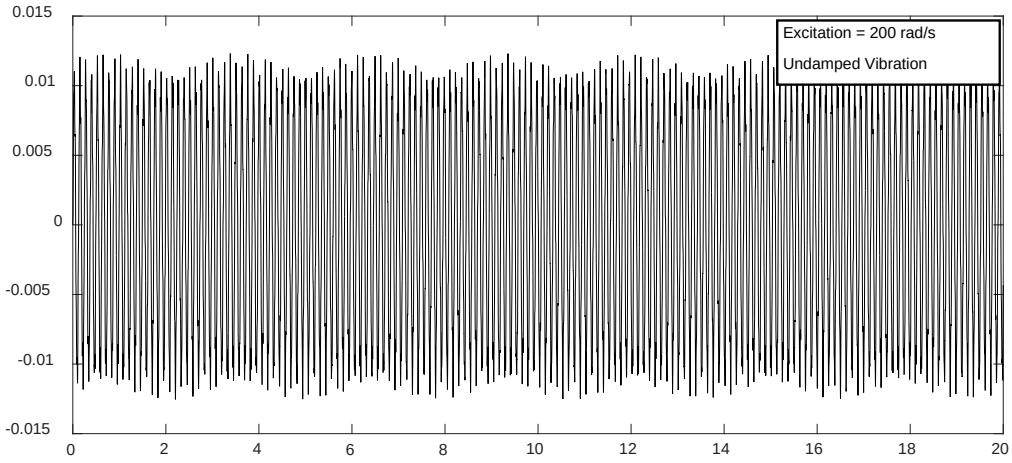

(b)

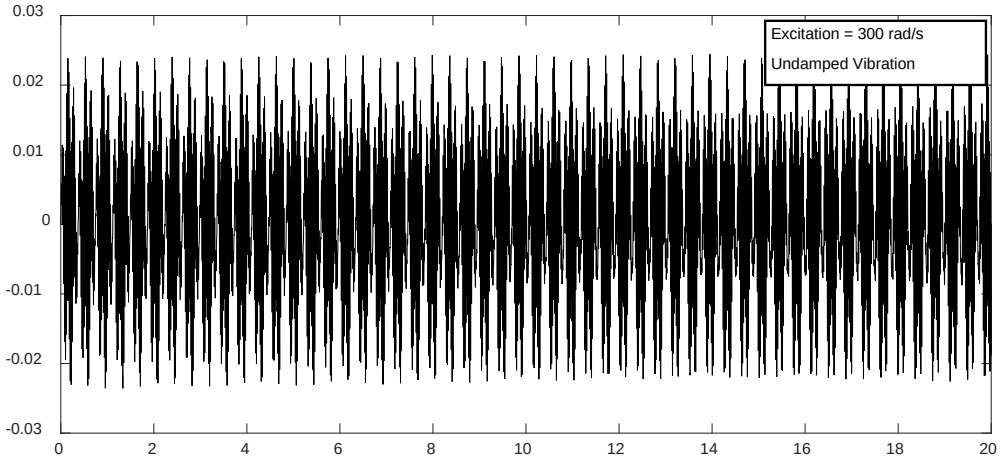

(c)

Figure 4. 6 - Dynamic responses at the free end of the cantilever beam, without damping under excitation frequencies of (a) 45 rad/s (b) 200 rad/s (c) 300 rad/s, and with the damping ratio of 0.01 under excitation frequencies of (d) 45 rad/s (e) 200 rad/s (f) 300 rad/s (continued to the next page..).

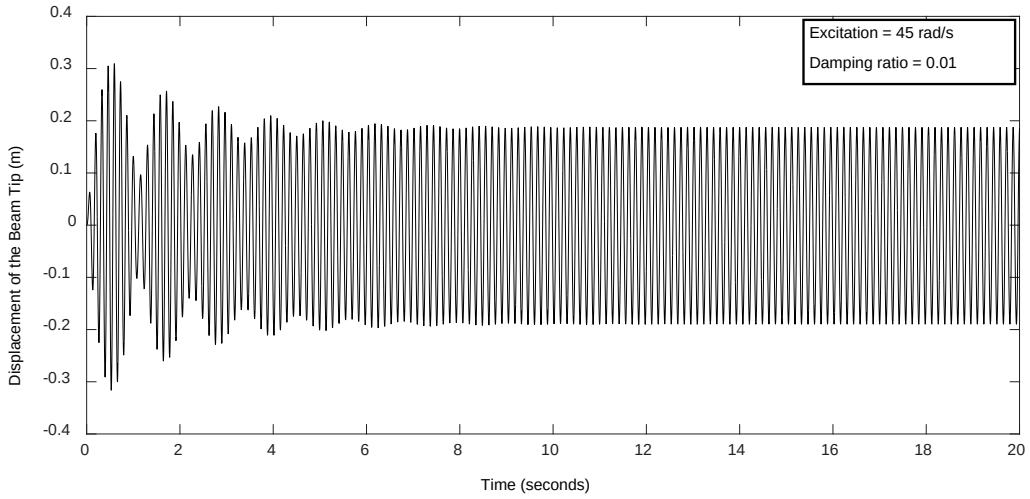

(d)

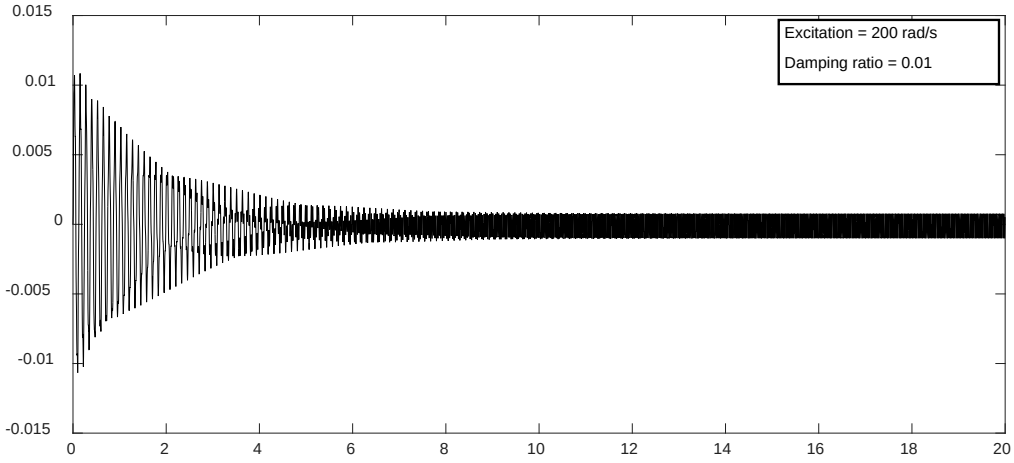

(e)

Figure 4. 7 - Dynamic responses at the free end of the cantilever beam, without damping under excitation frequencies of (a) 45 rad/s (b) 200 rad/s (c) 300 rad/s, and with the damping ratio of 0.01 under excitation frequencies of (d) 45 rad/s (e) 200 rad/s (f) 300 rad/s (continued to the next page..).

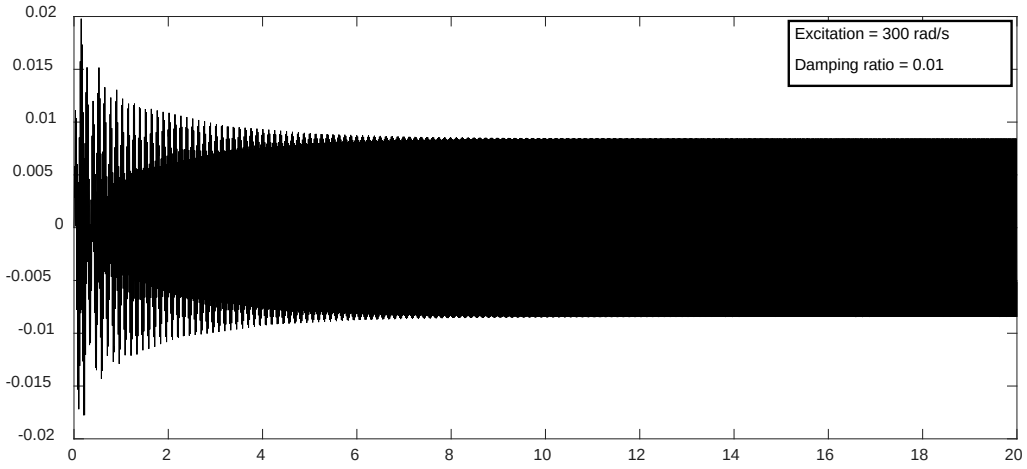

(f)

Figure 4. 8 - Dynamic responses at the free end of the cantilever beam, without damping under excitation frequencies of (a) 45 rad/s (b) 200 rad/s (c) 300 rad/s, and with the damping ratio of 0.01 under excitation frequencies of (d) 45 rad/s (e) 200 rad/s (f) 300 rad/s.

Figure 4.4 illustrates the undamped and damped vibration responses of the beam with 20% crack severity (20% crack depth percentage). The excitations of 45 rad/s and 300 rad/s are close to the first and second modal frequencies of the beam (refer Table 4.2). Beating phenomenon of the vibration response is expected and shown in Figure 4.4.(a) and (c). The corresponding damped responses under these two excitations given in Figures 4.4.(d) and (f) show the die down of the transient responses of the beam with beating and the process reaching the steady state after certain time. On the other hand, responses at 200 rad/s excitation frequency show the responses of the beam which are basically combined vibration responses of the first and the second modes. More discussions on dynamic responses relating to breathing of a cantilever beam and comparison of results from iterative method to the ones from finite element analysis (FEA) are found in [10].

The next sub-section introduces the results of crack identification using entropy as a quantification measure for the irregularities in the vibration signals.

4.3.2 Direct calculation of SampEn from the dynamic responses of the beam with a breathing crack

This section is dedicated to show the problems one has to face when the entropy is used alone for the breathing crack identification. Figure 4.5 illustrates the percentage increment of the SampEn of the cracked beams with respect to the healthy beam (the percentage SampEn of the healthy beam is 0%) and the percentage increment variation with different crack depth percentages.

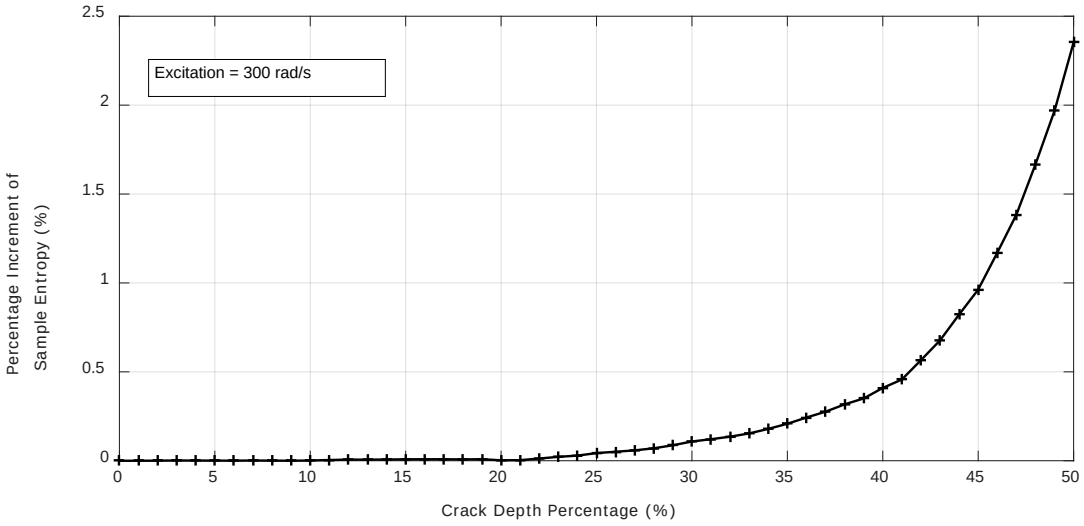

Figure 4. 9 - Variation of percentage increment of SampEn with different crack depth percentages.

The results depicted in Figure 4.5 are with the excitation of 300 rad/s. This represents the general variation of the SampEn values for other excitation frequencies studied. The embedding dimension ‘m’ and tolerance value ‘r’ for SampEn (refer equations (3.15) and (3.17) for the

respective parameters) are 2 and 0.2 of standard deviation (SD) of data respectively. 20,000 of data samples from steady state dynamic response is used for the entropy calculations. It can be seen from Figure 4.5, when the entropy calculations are directly employed on the dynamic signals, the method is fairly sensitive. It is seen that even at the 50% crack depth, the increment in the SampEn percentage is around just 2.5%. It can be concluded that the crack breathing effect on the vibration response of the beam structure is small with weak perturbations, which is not significant enough for the damage identification with entropy measurements. In practical applications, the small SampEn increment can be degraded due to presence of various noise components.

To improve the crack identification sensitivity of the proposed methodology using entropy, WT is then introduced to the crack identification process, and the results obtained using the WT as an add-in tool with entropy are presented in the next section. The word, ‘sensitivity’, represents the smallest identifiable crack depth percentage ratio to the thickness of the beam.

4.3.3 Entropy calculations with wavelet transformation as a data pre-processing add-in tool

In the current analysis, the damped-dynamic response generated by the iterative numerical method (introduced in Section 3.2) is first pre-processed by the WT, and then these transformed data is used for the entropy calculations (as described in Section 4.1). Then, the crack depth and SampEn value correlations are revealed.

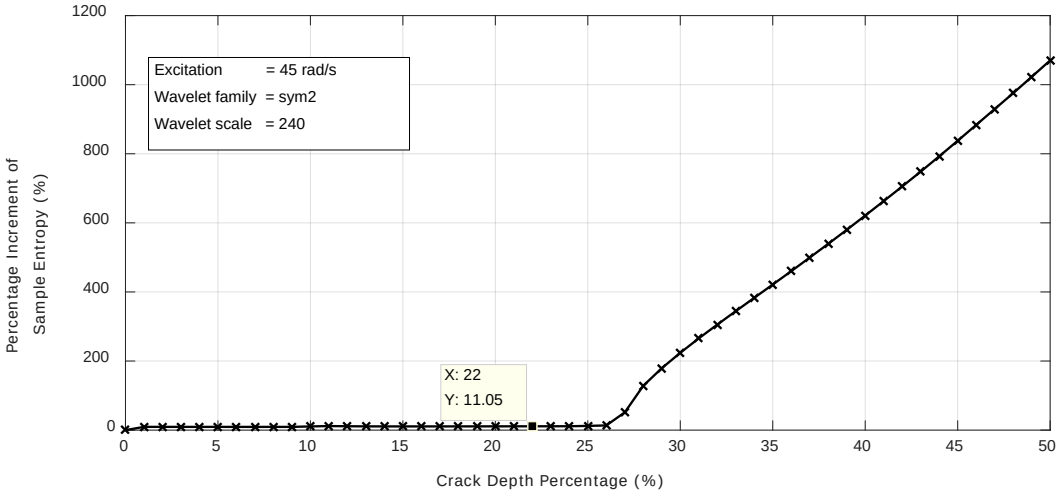
Excitation = 45 rad/s
Wavelet family = sym2
Wavelet scale = 240
X: 22
Y: 11.05
Percentage Increment of Sample Entropy (%)
Crack Depth Percentage (%)
0
200
400
600
800
1000
1200
0
5
10
15
20
25
30
35
40
45
50

(a)

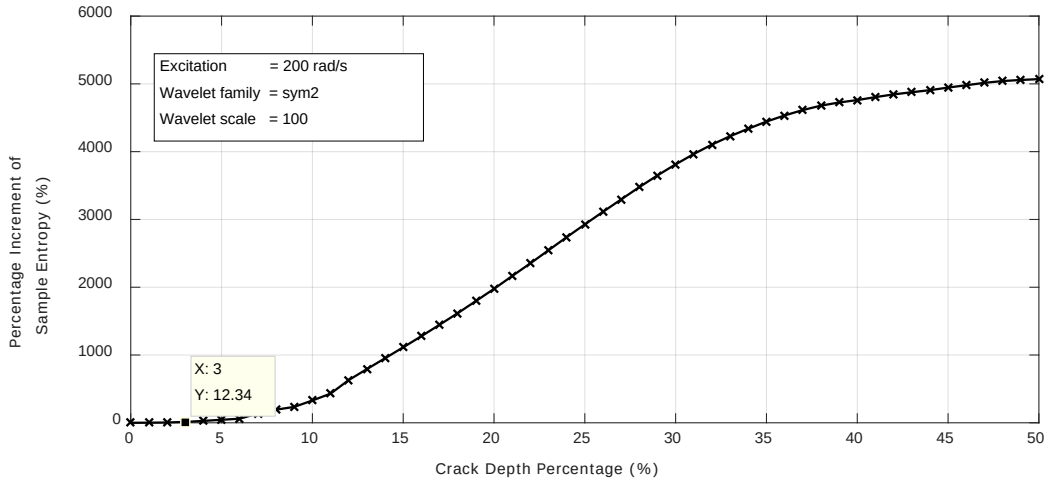
Excitation = 200 rad/s
Wavelet family = sym2
Wavelet scale = 100
X: 3
Y: 12.34
Percentage Increment of Sample Entropy (%)
Crack Depth Percentage (%)
0
1000
2000
3000
4000
5000
6000
0
5
10
15
20
25
30
35
40
45
50

(b)

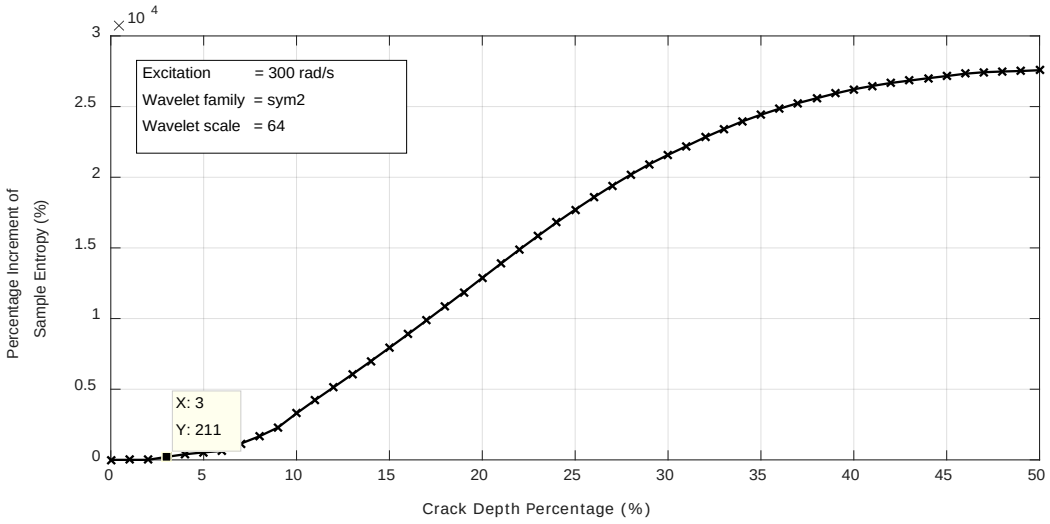

(c)

Figure 4. 10 - Variation of percentage increment of Sample Entropy of the Wavelet Transformed dynamic responses with different excitation frequencies, (a) 45 rad/s (b) 200 rad/s (c) 300 rad/s.

Figure 4.6 shows the variation of the percentage increment of the SampEn of the cracked beam with respect to healthy beam with different crack depth percentages. The parametric values of 'm' and 'r' for SampEn are 2 and 0.2 times SD of data respectively. 20,000 data points of the 'steady state' dynamic response is used and data is first sent through 'symlet2', which is the wavelet family used in MatLab® WT package. The WT is repeated for 9 times one WT after another WT manner, in order to have reasonable amplifications of the breathing effects. This is then followed by the SampEn calculations on the wavelet transformed data, and same number of data points (20,000 data points) is used in the entropy calculations. The variations of the percentage increment of SampEn with different crack depth percentages are found to be sensitive to the scaling parameter of WT. From Figure 4.6 it is observed that, low scaling parameters work well with vibration signals of higher excitation frequencies and vice-versa.

From Figure 4.6, dramatic increments in the sensitivity in crack identification can be seen showing much larger entropy value increments due to the crack breathing effect after the introduction of WT. In Figure 4.6.(a), for the excitation of 45 rad/s, the crack depth percentage varies from 0% (healthy beam) to 50%, and SampEn percentage increment varies from 0% to around 1050%. During the analysis of the simulation results, it is assumed that the cracks are only identifiable when the percentage increments of entropies due to the crack effect are more than 10% compared to the healthy beam. This is to keep some safe margin for the presumed degradation of the results of the proposed crack identification method, due to the inevitable environmental noises during the practical operation. With this assumption, from Figure 4.6.(a), it is noted 22% of crack depth percentage can be detected with 11% SampEn increment compared to the healthy structure. Then the increment value increases slightly until the crack depth percentage of 26% where it shows 13% of SampEn increment compared to the healthy beam, and then the increment value increases almost linearly with the increment of the crack depth. From Figures 4.6.(b) and (c), similar trends can be found, but much higher damage identification sensitivity can be realized with higher excitation frequencies. In Figure 4.6.(b), With the 200 rad/s excitation, SampEn percentage increment is about 5000% at 50% crack depth, and Figure 7(c) shows around 27,000% increment with 300 rad/s excitation frequency at 50% crack depth. Both Figures 4.6.(b) and (c) show more than 10% increment in SampEn compared with the healthy structure at an initial crack with 3% depth percentage. Again, the 300 rad/s shows much higher SampEn increment (211%) than 200 rad/s case (12%) at 3% of crack depth percentage. The reasons for the change in SampEn increment with different crack depth percentages and the effect of the excitation frequencies on the damage identification sensitivity are explained in the following paragraphs.

According to equations (3.6) and (3.7), larger crack depths in the beam lead to more significant stiffness reductions and larger slope differences at the two sides of the crack when the crack opens. Therefore, larger cracks result in more significant changes in the structure response during the vibration with the crack breathing. This is evident in Table 4.2, where it is noticeable that the difference in the modal frequencies of the healthy beam and the damaged beam stages increases as the crack depth increases; for example in the first mode of vibration, this particular difference increases from 0.104 rad/s to 3.048 rad/s when the crack depth percentage increases from 10% to 50%. The structural change during the vibration induces more significant perturbations in the vibration signal and hence leads to larger entropy values. As it is seen in the previous section (Section 4.3.2), the perturbations are not substantial enough to make significant changes in the SampEn values compared to the healthy beam. However, after these perturbations are amplified by WT, it is evident from Figure 4.6 that entropy calculations are much more sensitive to the changes of the crack depths yielding much more significant SampEn increment. The amplification of perturbations by WT makes the proposed methodology to have superior sensitivities in crack identification in certain frequencies around 200~330 rad/s than the frequencies around 40~200 rad/s. The reasons for better sensitivities in crack identification at higher frequencies of excitations compared to lower excitations are explained in the following paragraph.

Higher excitation frequencies lead the vibration of the beam to be dominated by higher vibration modes of the beam. Since the crack is closer to the fixed end of the beam, which is the most practical location for occurrence of fatigue cracks; the higher normalized vibration mode shapes provide higher curvatures distribution at the crack position compared with the normalized lower mode shapes which are dominant in lower excitation frequencies. These larger curvatures

at the crack position give rise to more significant stiffness reduction at the crack, which result in more significant changes in the structure and its response during the vibration with the crack breathing, even at the initial stages of the crack. This is again evident in Table 4.2, higher modal frequency difference between healthy and the damaged stages is found for higher natural modes of the structure with any given crack severity level; if 10% of crack depth is considered this difference increases as 0.104, 0.608 and 1.589 rad/s for the first, second and the third vibration modes, respectively. Therefore, with constant excitation amplitude, as the excitation frequency increases, the vibration responses with higher vibration modes lead to more significant perturbations in the vibration signal. In addition, in a similar cantilever beam study with a breathing crack, Wu [10] has observed dramatic non-linear increment in the equivalent breathing frequencies with the increment of the excitation frequency closer to the second natural frequency of the beam. Higher breathing frequencies impose more perturbations in the vibration signal within a certain period leading to higher entropy increments. Therefore, higher entropy percentage increments, which ultimately result in better crack identification sensitivities, are induced by higher excitation frequencies.

Even though the SampEn shows higher sensitivities (once combined with WT) to the crack induced perturbations, one thing noticed in the analysis is their long computational times. This would be a problem during implementation of the proposed work for a real application. Therefore, as the next step, QASE is used to improve the computational efficiencies of the crack identification process, and this is covered in the next sub-section.

4.3.4 Speed-up of crack identification process with QASE

QASE is an entropy measure, which is developed by keeping in mind of higher computational efficiencies. So, it is intended to use QASE together with SampEn to speed-up the crack identification process. Figure 4.7 compares the computational times for SampEn and QASE, and reveals the huge computational time gains of QASE over SampEn.

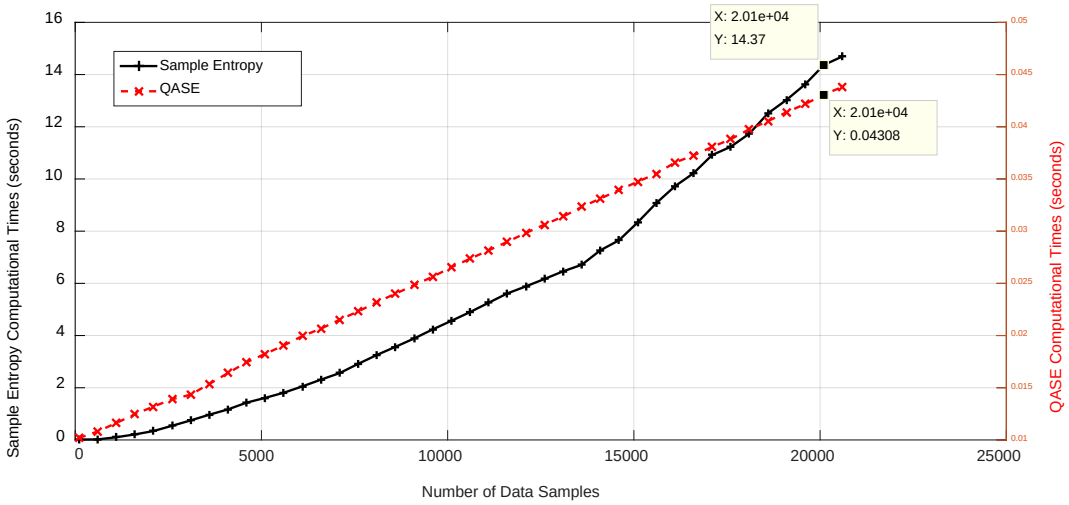

Figure 4. 11 - Variation of computational times of SampEn and QASE with different number of data samples.

The computations are done using an Intel® Core i5 3.30 GHz personal computer with 8 GB of random-access memory (RAM) without running any other substantial program in background. In Figure 4.7, X-axis shows the number of data samples used for the entropy calculations. At 20,000 data samples, which is the number of data samples used throughout the analysis; QASE takes 0.04 seconds for the calculations and SampEn needs 14 seconds. QASE is about 325 times faster than SampEn at 20,000 data samples. This computational gain can be used to improve the computational speed of the crack identification process as it is explained in the following paragraphs.

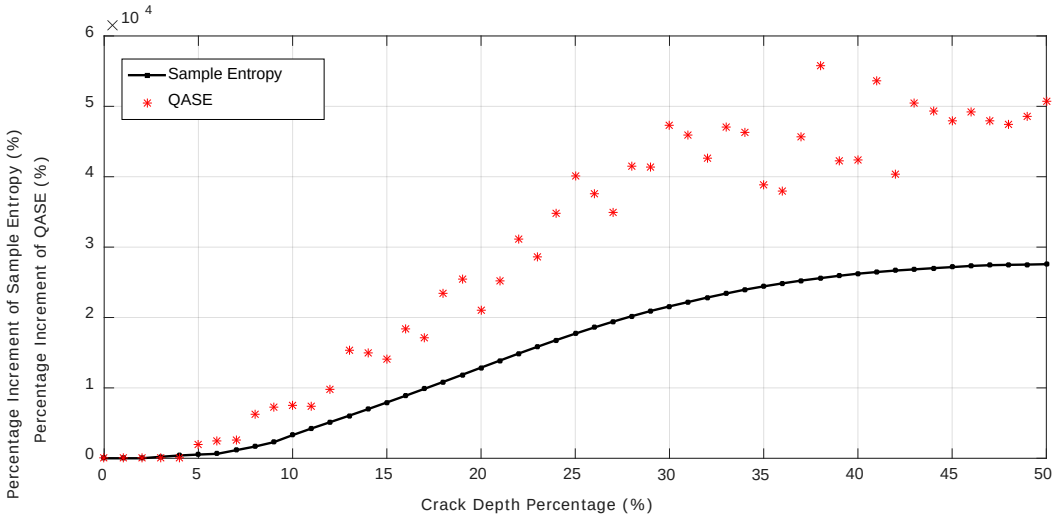

Figure 4. 12 - Variation of percentage increment of SampEn and QASE with different crack depth percentages with excitation frequency of 300 rad/s.

Figure 4.8 shows the variation of both percentage increments of SampEn and QASE with different crack depth percentages changing from 0% to 50%. The Excitation frequency is 300 rad/s and the same WT is used prior to the entropy calculations (SampEn variation is same as the illustration in Figure 4.6.(c)). The parametric values of 'm' and 'r' for both SampEn and QASE are 2 and 0.2 times SD of data, respectively. Figure 4.8 shows around 1900% QASE increment at just 5% crack depth compared with the healthy beam, although the QASE variation with different crack depths is not as smooth as SampEn. . The non-smooth behavior of QASE is due to the approximation technique called 'relative coarse quantization of data', which is used by the QASE to approximate SampEn.

The non-smooth variation of the QASE disqualifies it as the major entropy measure to accurately quantify the crack depth, but its computational efficiency improvement can still benefit the proposed work for the high sensitivity damage detection. It is decided to use QASE as the initial crack detector, due to its better computational efficiencies and ability to display

considerable percentage entropy increments compared with the healthy structure especially at initial crack depths. Then once a crack is detected by QASE values, SampEn is employed to further evaluate the crack. This approach leads to faster crack detection with QASE, and accurate damage predictions with SampEn.

Up to this section of the thesis, everything has been analyzed in a sense of pure computational environment, without considering any outside noises, which are inevitable in practical testing. Therefore as the next step, the effect of noisy-vibration signals on the current methodology is studied.

4.3.5 Impact of observational noise on breathing crack identification

The impact on the proposed method by the presence of noise in the vibration signal is studied by adding Gaussian white noise to the dynamic response of the beam, which has been illustrated in Section 4.3.1. This noisy data represents real vibration data collected from a practical vibration testing using a data acquisition system.

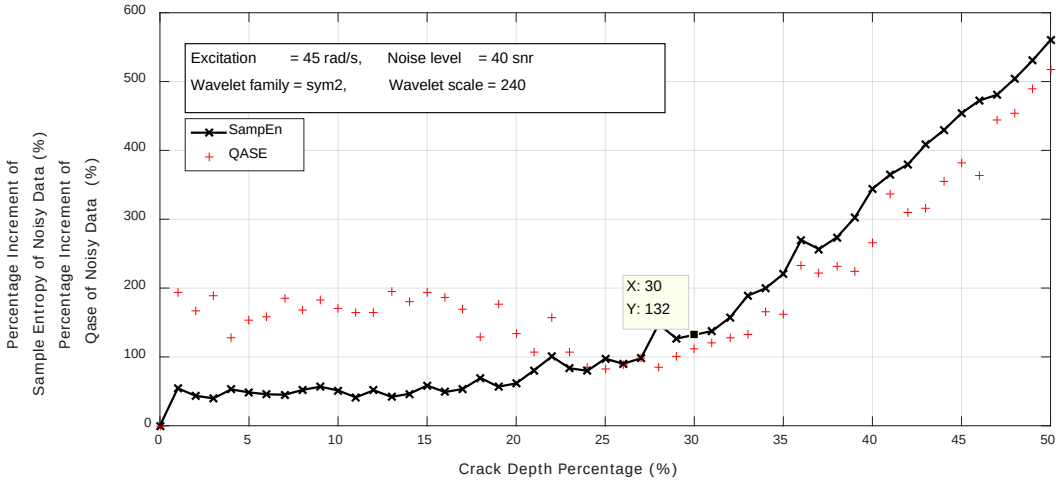

Figure 4. 13 - Variation of percentage increment of SampEn and QASE with different crack depth percentages for noisy data with 40dB SNR of noise level (the excitation frequency is 45 rad/s).

Figure 4.9 shows the averaged variation of percentage increments of SampEn and QASE with different crack depth percentages for noisy data for ten runs; the excitation frequency is 45 rad/s and the noise level is 40dB of signal-to-noise ratio (SNR). SNR is measured using the logarithmic decibel scale of the ratio between the root sum square (RSS) of signal to RSS of noise. The averaging of the values from the ten runs is obtained by taking the linear average of percentage entropy increments compared to the healthy beam value. Each run imposes randomly created noise on the dynamic signal; therefore slightly different results are obtained in each run for the percentage entropy increments. The averaging is more realistic with real world application of the proposed method. The excitation frequency of 45 rad/s is chosen for the study, because in Section 4.3.3, it can be seen that the crack identification results for lower excitation frequencies are not as good as for higher excitation frequencies, therefore study of the worst scenario in depth is given more importance.

From Figure 4.9, it can be seen that the range of the percentage increment of SampEn compared with the healthy beam is from 0% to around 560%, when crack depth increases from 0% to 50%; for QASE this range of the percentage increment is from 0% to about 517% (the word ‘range’ stands for the amount of variation in the entropy increment compared with the healthy structure, when the crack depth percentage varies from 0% to 50% of the beam thickness). It is noted that, for the noiseless scenario given in Figure 4.6.(a), the particular range of the percentage increment is from 0% to around 1050% for SampEn. During the analysis it is noted that for QASE, the entropy increment range is from 0% to around 1080% as the crack depth percentage varies from 0% to 50%. The sensitivity of crack detection for noiseless scenario is 22% crack depth of total beam thickness (with 11% increment of SampEn), and for the 40dB SNR scenario the sensitivity has dropped down to 30% (with 132% increment of SampEn). The reason behind the reduction of the sensitivity due to the presence of noise in the vibration signal is explained in the next paragraph.

For the excitation of 45 rad/s, for the noiseless dynamic responses, it is observed that both SampEn and QASE are not significantly sensitive to the crack depth percentages until around 26% compared to their dramatic increments for the rest of the crack depth percentages from 26% to 50%. Therefore, once the noise is present in the dynamic signal, the noise is more dominant than the crack breathing effect for the crack depth percentages of 0% to 26%. This leads to more fluctuations in the percentage entropy increments in both SampEn and QASE in that crack percentage region causing a reduction in the sensitivity of crack detection.

The results obtained in this section for noisy dynamic signals can be compared with real experimental results obtained for a similar beam setup. The next section is dedicated for this purpose.

4.3.6 Experimental results and comparison with the numerical values

In this section, the numerically simulated results obtained for noisy dynamic signals (40 SNR) for a lower excitation (45 rad/s) in the previous sub-section are compared with the experimental results. The experimental results are obtained using the experimental setup described in Section 4.2.

The three experimental aluminum alloy cantilever beams, i.e. healthy beam, 25% crack depth percentage beam and 50% crack depth percentage beam, are excited with a frequency of 5.92 Hz which is close to the first modal frequencies of the three beams. Measurements include raw acceleration-time data for the three beams. Figure 4.10 shows a snapshot of the time series data for 50% crack depth percentage beam.

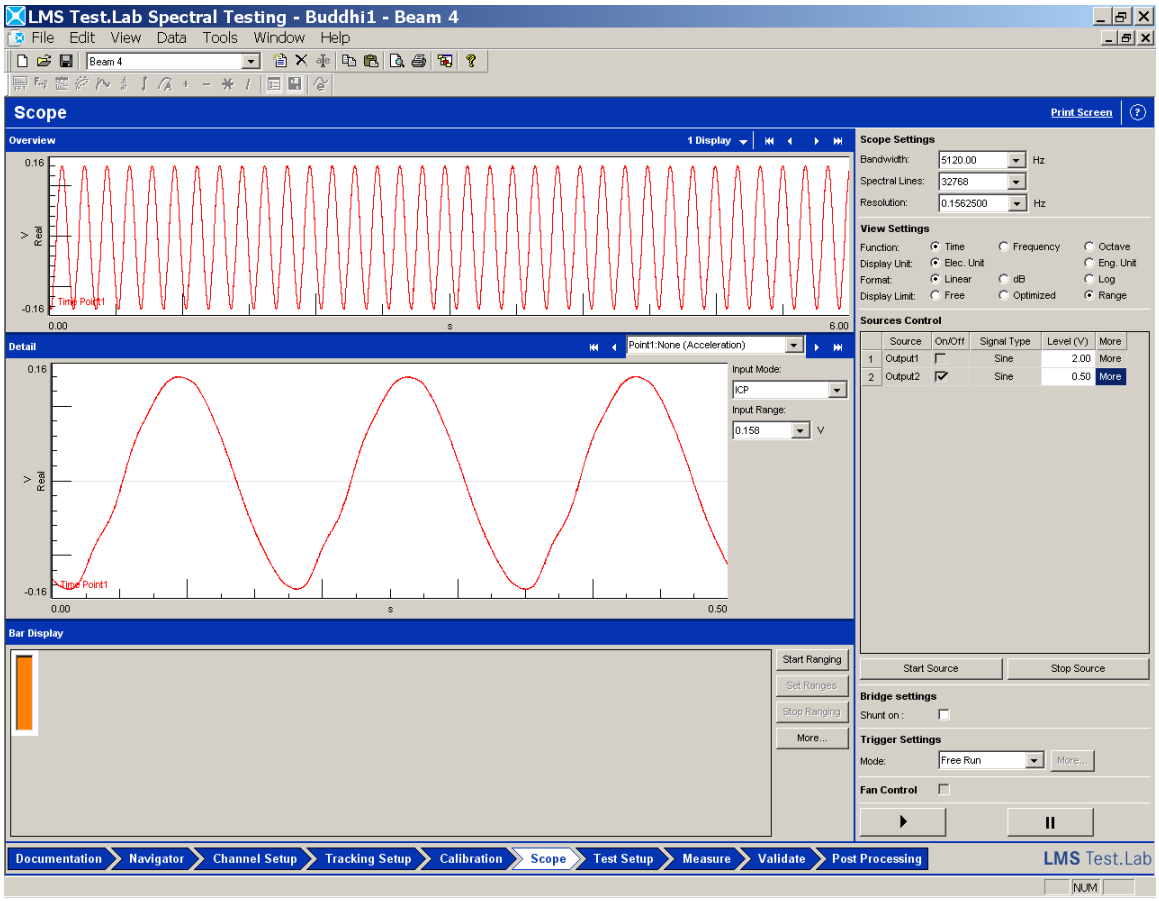

Figure 4. 14 - Graphical user interface of the data acquisition system for the experimental setup (time series is shown for the beam with 50% crack depth percentage).

From the acceleration-time data collected for the three beams, 20,000 data is selected for further analysis. These data sets are then transformed using WT (same WT parameter values are used as the numerical simulation; i.e. scale is 240 and WT is done for nine consecutive times). The transformed data is then analyzed using SampEn and QASE while keeping the entropy parameter values same as the numerical analysis (m = 2 and k = 0.2). This procedure is repeated for ten times for all three beams using ten different data sets collected in different experimental run initiations. Table 4.3 compares the experimental and numerical results of linearly averaged (using ten runs) SampEn and QASE percentage increments for 25% and 50% crack depth

percentage beams compared to the healthy beam. Numerical results for 25% and 50% crack depth percentage beams are obtained from the previous section.

Table 4. 3 - Averaged percentage increment of SampEn and QASE for the beams of 25% and 50% crack depth percentages.

		25% crack depth percentage beam		***50 % crack depth percentage beam***	
		Averaged percentage increment of entropy compared to the healthy beam (%)	Standard deviation	Averaged percentage increment of entropy compared to the healthy beam (%)	Standard deviation
SampEn	Numerical method	97.5	52.4	560.4	14.3
	Experimental method	94.9	66.3	753.5	11.5
	Percentage difference of two methods (%)	2.7		25.6	
QASE	Numerical method	83.1	63.5	517.5	21.2
	Experimental method	87.4	62.6	633.8	15.3
	Percentage difference of two methods (%)	4.9		18.3	

From Table 4.3 it can be seen that numerical and experimental results have a good match with each other for both crack depth percentages. For the 25% crack depth percentage beam, SampEn increment difference between numerical and experimental methods is as small as 2.7% while QASE shows a difference of 4.9%. On the other hand, for 50% crack depth percentage beam,

numerical and experimental values of SampEn shows a difference of 25.6% and QASE shows 18.3% for the respective difference.

In addition, from Table 4.3, it is also noted that the standard deviation values are comparatively larger for 25% crack depth percentage beam over the 50% crack depth percentage beam for both numerical and experimental results. This result further strengthen the point that, for the crack depth percentage region from 0% to around 26%, both SampEn and QASE are not very sensitive to the crack breathing for lower excitation frequencies due to the dominance of the noise.

4.4 Summary

In this chapter, the proposed breathing crack identification technique is employed to study the breathing crack cantilever beam (the case study) under sinusoidal excitation. At the beginning of the chapter, the overall crack identification methodology is elaborated followed by the in-house experimental setup. Then a detailed results and discussions section is given for both numerical simulations and experimental studies under several sub-sections. The sub-sections consecutively covered the followings: the dynamic response generation using the iterative numerical model; this is to illustrate the accuracy of the crack modeling technique which is essential in developing any damage identification methodology. Then the next sub-section revealed the problem related to standalone usage of entropy in crack identification, which is followed by the introduction of WT in to the crack identification process. This sub-section revealed high sensitivity crack identification for small and initial cracks with only 3% of the beam thickness with more than 200% increment in SampEn compared with the healthy beam, and it is also shown comparatively lower

crack identification sensitivities for lower excitations which are around the first modal frequency of the cantilever beam. Then QASE is introduced to show the possible computational gains in the crack identification process, which showed large computational gains over SampEn. As a final step in numerical simulations, the effect of observational noise is studied which is inevitable in real breathing crack identifications. Then, the results and discussion section is ended with a comparative study using numerical simulation results for noisy vibration data, and experimental results, in which a good agreement between two methods were observed.

The final crack identification sensitivities rely on the parametric values of both entropy and WT calculations. As it is mentioned in this chapter, SampEn uses two parametric values; they are the embedding dimension ‘m’ and the positive constant of ‘k’ (this value varies the tolerance value ‘r’). On the other hand, WT also uses two parameters in its calculations; those are the ‘WT scale’ and the ‘WT repetitions’. In the next chapter, these four parameters are optimized to achieve better crack identification sensitivity for lower excitation frequencies, the frequency level which showed comparatively lower performances as it is observed in this chapter.

Chapter 5

Parametric Optimization of Sample Entropy and Wavelet Transformation

In the previous chapter, it was noted that the entropy calculation and WT results depend on four parameters: m, k, WT scale and WT repetitions, which will affect the damage identification accuracy and sensitivity. This chapter focuses on the improvement of the damage identification sensitivity by optimizing theses parametric values of SampEn and WT. In the previous chapter it was noted that (in Section 4.3.3) crack identification sensitivity for lower excitation frequencies (excitation frequencies close to the first modal frequency of the structure) was less compared to the higher excitation frequencies of the structure. In other words, the crack identification sensitivity for 45 rad/s excitation was lower compared to the higher excitations of 200 rad/s and 300 rad/s. Therefore, a parametric study is carried out to improve the crack identification sensitivity for the 45 rad/s excitation frequency by optimizing the four parameters in SampEn and WT.

In Section 5.1 the experimental setup is given and Section 5.2 covers the detailed parametric optimization process with the corresponding numerical results at each optimization stage. At the

end of that section, the numerical and experimental results are compared and discussed to verify the parametric optimization.

5.1 Experimental setup

It should be noted that, in this experimental analysis, the same experimental setup is used which is described in Section 4.2 in the previous chapter. But, for this analysis, only the healthy beam and the 25% crack depth beams are analyzed. Figure 5.1 illustrates the schematic arrangement of the bonded beam pieces for constructing the beam with a 25% crack depth percentage.

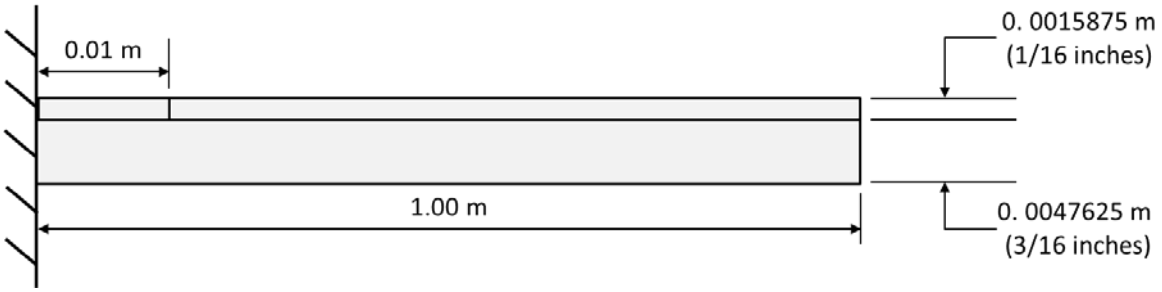

Figure 5. 1 - Schematic diagram of the constructed test beam for 25% crack depth percentage.

Figure 5.2 shows the experimental setup for obtaining the dynamic response from the 25% crack depth percentage beam. Both healthy and 25% crack beams are sinusoidally excited.

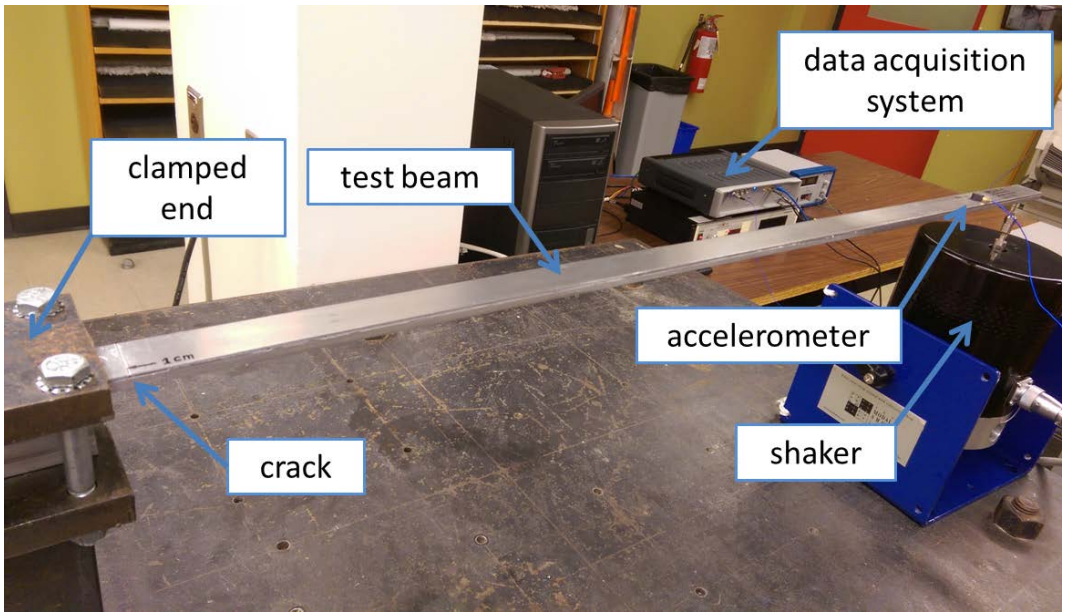

(a)

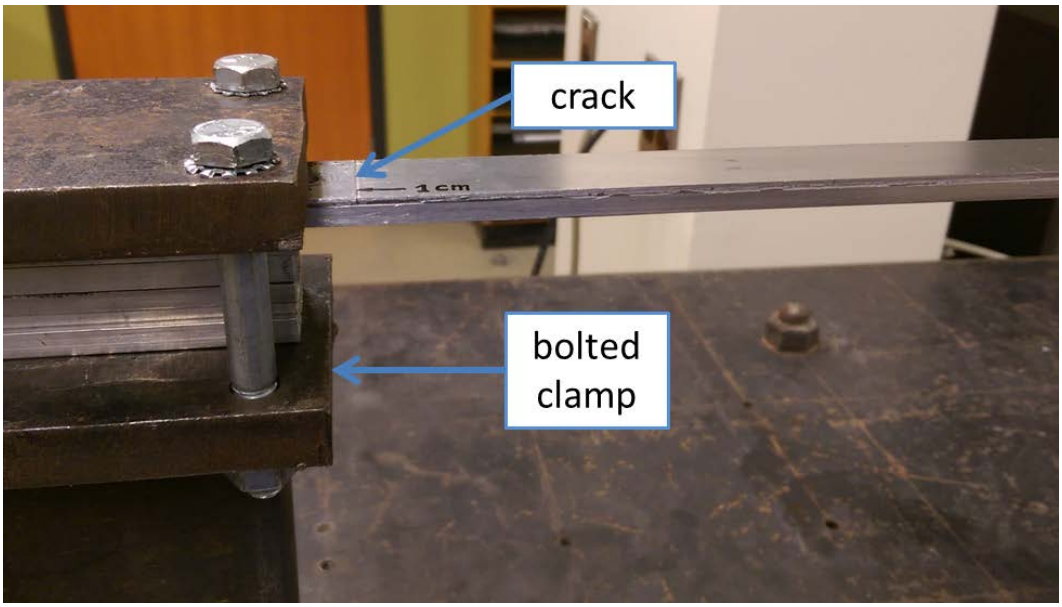

(b)

Figure 5. 2 - The experimental setup for obtaining dynamic responses of damaged and healthy aluminum alloy cantilever beams (a) the whole setup for testing of the beam with 25% crack depth percentage (b) the clamped end of the beam.

5.2 Results and discussions

In this section, first, the numerical simulation results (for this, the iterative mathematical model is used to generate the vibration signals and it should be noted that no noise is added to the signals) are improved by the parametric optimization of SampEn and WT, and the corresponding crack identification sensitivities are found. Then once the optimum parametric values are found for SampEn and WT, these values are used to calculate the experimental results for the considered excitation. In the final sub-section these numerical and experimental results are compared so as to validate the parametric optimization. This parametric optimization is done in two individual steps; first the parameters of SampEn are optimized and WT parametric optimization is followed after that in the second step.

5.2.1 Parametric optimization of SampEn

In the previous chapter, the parametric values used for SampEn to analyze 45 rad/s excitation are; m is 2 and k is 0.2. And the parametric values for WT are; scale is 240 and WT repetitions are 9. In this study, to improve the crack identification sensitivity at 45 rad/s, as the first step, the parametric values of SampEn are optimized while keeping the WT parameters in their non-optimized values (i.e. scale at 240 and WT repetitions at 9). This is done using a traverse optimization algorithm; the flowchart of the algorithm is given in Figure 5.3. The algorithm is implemented using MatLab® software package and the algorithm is explained in the following paragraphs.

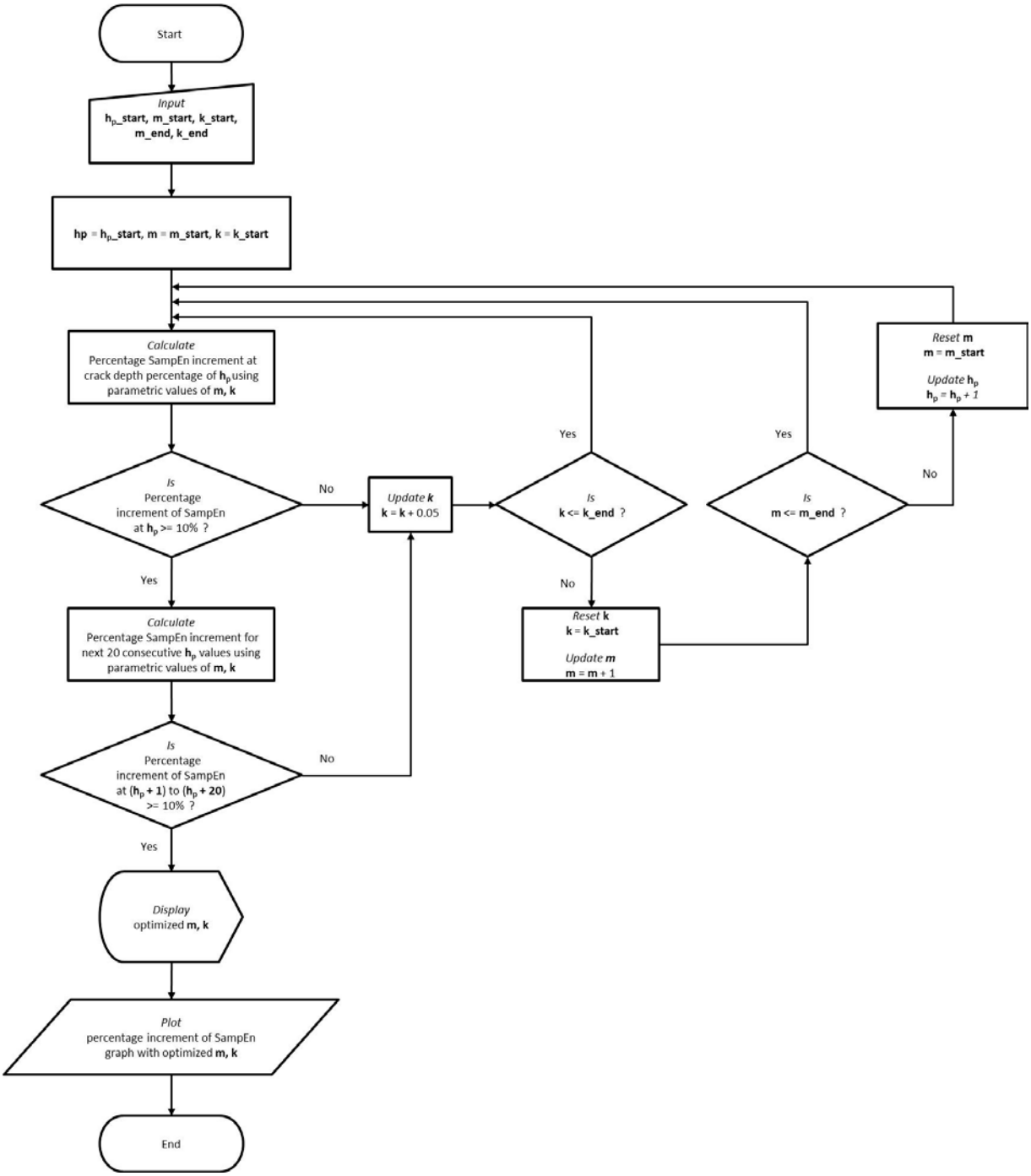

Figure 5. 3 - Flowchart of the Traverse Optimization Algorithm for optimizing SampEn parametric values.

First, the ranges for the parametric values of m and k are pre-defined. For m, the range is selected from 2 to 10 with increments of 1. Therefore in Figure 5.3, m_start (starting value of m) is 2 and m_end (ending/ limiting value of m) is 10. m_end is chosen such that, higher the value of m, higher the computational time will be. For example, for a value of 2 for m, SampEn takes around 14 seconds to compute the calculation for 20,000 data samples (refer Section 4.3.4). Then, for a value of 4 for m, this time will be doubled approximately. Therefore, a value of 10 as the limiting value for m is considered more appropriate over a higher value than 10. For k, k_start is 0.1 and k_end is 1 with an increment is 0.05. Once these ranges are set for the parametric values of SampEn, the algorithm requires a starting value for the crack depth percentage, h_p_start. During the analysis, this h_p_start is set as 3%, because that's the best crack identification sensitivity achieved for higher excitation frequencies in the previous chapter.

Then, the algorithm calculates the percentage increment of SampEn at h_p_start crack depth percentage, initially using m_start and k_start values as the parametric values. If the percentage increment of SampEn is less than 10% at h_p_start crack depth percentage, the m and k values are incremented accordingly until this condition is satisfied. If this condition is satisfied for a certain value of m and k, at h_p_start crack depth percentage, then the same condition (i.e. whether percentage increment of SampEn is higher than 10%) is checked for the next 20 consecutive crack depth percentages, in-order to achieve a smooth and more practical SampEn percentage increment for the next consecutive crack depths. If this is satisfied, then the corresponding m and k values are displayed and the variation of percentage increment of SampEn with 0% to 50% of crack depth percentages is plotted (a plot similar to Figure 4.6). If the percentage increment of SampEn values are less than 10% for the whole range of m and k value for the crack depth percentage of h_p_start, then the crack depth percentage (h_p) is incremented by one

(h_p=h_p_start+1). Then the same checks are done for the updated crack depth percentage as it is described earlier in this paragraph. The algorithm goes from one crack depth percentage to the next crack depth percentage while looping through the parametric values of m and k, looking for a better plot with better crack identification sensitivity. Due to this traversing optimization nature of the algorithm, the name 'traverse optimization algorithm' is coined by the authors. Figure 5.4 shows the resultant graph from the algorithm.

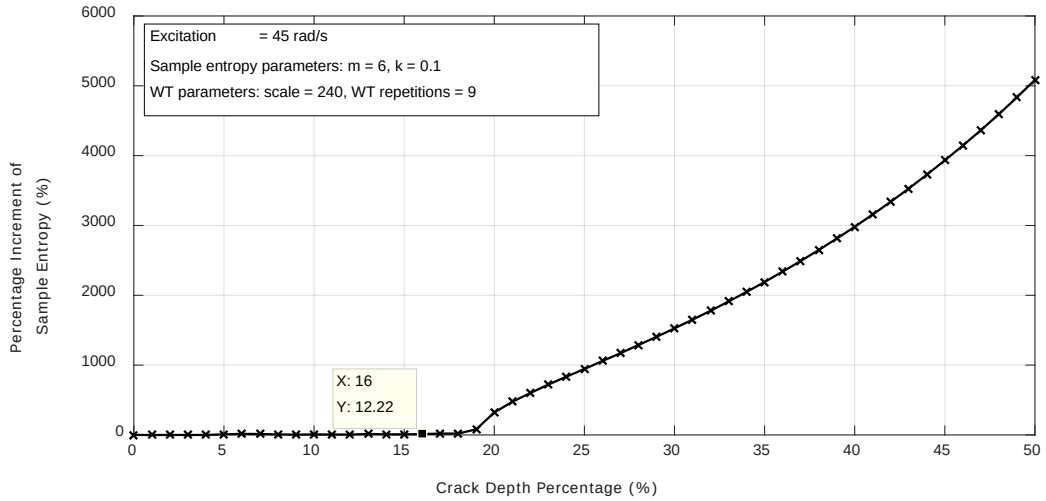

Figure 5. 4 - Variation of percentage increment of sample entropy of the wavelet transformed dynamic response for the excitation frequency of 45 rad/s with optimized parametric values of SampEn.

The algorithm produced final optimized parametric values for m and k are 6 and 0.1 respectively. It can be seen from Figure 5.4, for the new optimized parametric values of m and k, the crack identification sensitivity has been improved to 16% crack depth percentage with a 12% percentage increment of SampEn with respect to the healthy beam. Before this parametric optimization for SampEn, this crack identification sensitivity was 22% with 11% in the percentage increment of SampEn. In addition, from Figures 4.6.(a) and 5.4, it should be noted

that the percentage increment of SampEn values at 50% crack depth percentage has been improved from around 1000% to around 5000% with the parametric optimization.

After this parametric optimization of SampEn, parametric optimization of WT is considered. This study and results are given in the next sub-section.

5.2.2 Parametric optimization of WT

WT has two parameters; viz. WT scale and WT repetitions. During the analysis it is found that, these parameters have a huge impact on the final crack identification sensitivity. The parametric optimization of WT is done as the following paragraphs explain.

First, the percentage increment of SampEn variation with respect to WT scale and WT repetitions are observed using a three dimensional plot (3D plot). The 3D plot is graphed for the crack depth percentage which is the crack identification sensitivity achieved with parametric optimization of SampEn in the previous sub-section (i.e. 16% crack depth percentage). This 3D plot is shown in Figure 5.5.

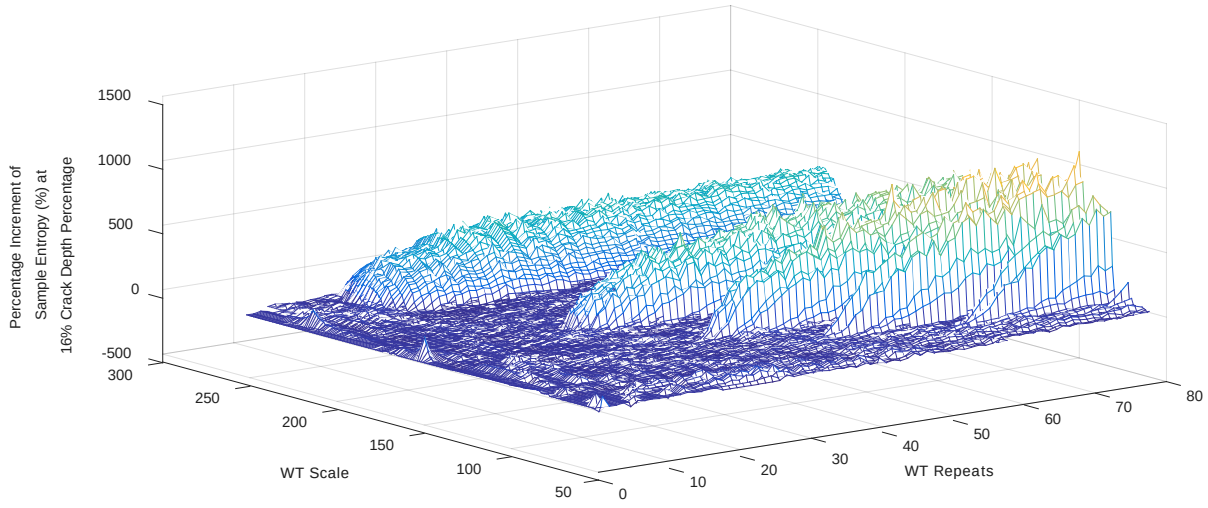

Figure 5. 5 - Variation of percentage increment of sample entropy of the wavelet transformed dynamic response for the excitation frequency of 45 rad/s at 16% crack depth percentage.

It can be seen form Figure 5.5 that percentage increment of SampEn (at 16% crack depth percentage) has some hills and valleys with the variation of WT scale and repetitions. Then, for the parametric optimization process, the WT scale and repetition ranges corresponding with the hills of the 3D plot are selected. As the next step, these ranges are given to another traverse optimization algorithm, which is similar in optimization procedure to the algorithm explained in previous sub-section. In order to refrain from repeating similar explanations, this algorithm is not explained in details in this thesis. This algorithm optimizes the WT scale and repetition values such that the crack identification sensitivity is further improved. After the analysis, the algorithm produced final optimized parametric values for WT scale and WT repetitions as 240 and 40 respectively. The graph with improved crack identification sensitivity with optimized WT parametric values is shown in Figure 5.6

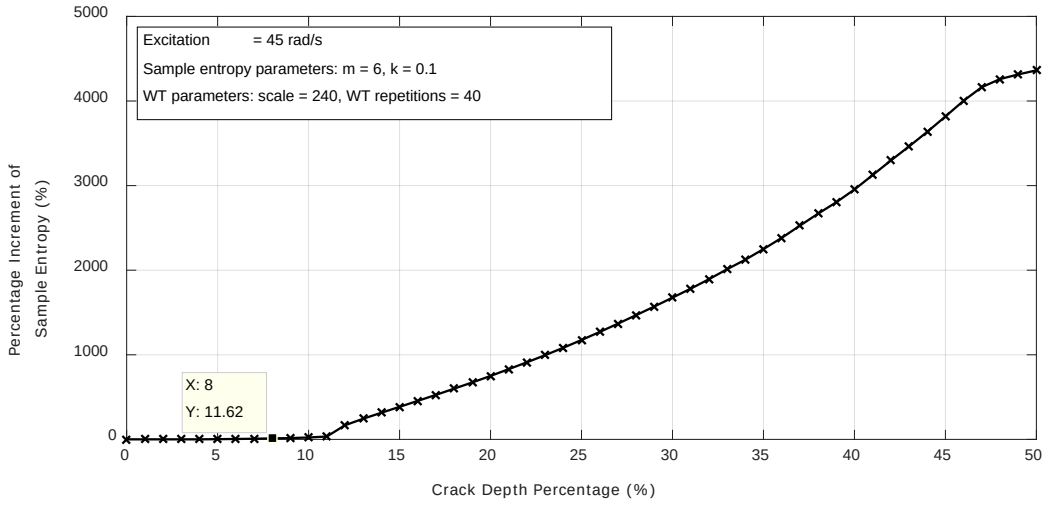

Figure 5. 6 - Variation of percentage increment of sample entropy of the wavelet transformed dynamic response for the excitation frequency of 45 rad/s with optimized parametric values of SampEn and WT.

Figure 5.6 shows that the new crack identification sensitivity is 8% crack depth percentage with an 11% percentage increment of SampEn with respect to the healthy beam. The crack identification sensitivity has been improved from 22% (for the non-optimized parametric values of both SampEn and WT, which is the original value shown in Figure 4.6.(a)) to 8% of crack depth percentage as a result of the final parametric optimization of both SampEn and WT.

Then, as the last step in this chapter, the numerical results for percentage increment of SampEn values at 25% crack depth percentage values obtained from Figure 4.6.(a) (i.e. result from non-optimized parametric values) and Figure 5.6 (the final result from optimized parametric values) are compared with the experimental results for the 25% crack beam. These comparisons are given in the next section.

5.2.3 Experimental verification of parametric optimization

In this section, the numerical results for percentage increment of SampEn using optimized and non-optimized parametric values for both SampEn and WT are compared with experimental results to verify the desired outcomes from the parametric optimization. The experimental results are obtained using the experimental setup described in Section 5.1.

The two experimental aluminum alloy cantilever beams, i.e. healthy beam and 25% crack depth percentage beam are excited with a frequency of 5.92 Hz which is close to the first modal frequencies of the two beams. Measurements include raw acceleration-time data for the two beams. From the acceleration-time data collected for the two beams, 20,000 data is selected for further analysis. Then these data are analyzed for the percentage increment of SampEn with the two different settings of the parametric values. The first setting is the non-optimized parametric values: m = 2, k = 0.2, WT scale = 240 and WT repetitions = 9. And the second setting is the optimized parametric values: m = 6, k = 0.1, WT scale = 240 and WT repetitions = 40. Then these results are compared and shown in Table 5.1.

Table 5. 1 - Comparison of numerical and experimental results for percentage increment of SampEn on the beam of 25% crack depth percentage with optimized and non-optimized parametric values.

Method	***Percentage increment of SampEn at 25% crack depth percentage compared with the healthy beam (%)***	
	Using non-optimized parametric values of SampEn and WT *(m=2, k=0.2, WT scale=240, WT repetition=9)*	Using optimized parametric values of SampEn and WT *(m=6, k=0.1, WT scale=240, WT repetition=40)*
Numerical Method	12	1175
Experimental Method	9	59

Table 5.1 reveals that both numerical and experimental results (12% and 9%) are in good agreement with each other for the percentage increment of SampEn at 25% crack depth percentage with non-optimized parametric values of SampEn and WT. On the other hand, with the optimized parameters, significant improvement of the detection sensitivity is noticed for the 25% crack from both simulation and experimental studies. The SampEn increments of the vibration response due to the crack are enhanced to 1175% and 59% in the simulation and experiment results, respectively. It is noted that the experimental result is lower than the numerical result by a considerable value. This is due to the inevitable presence of environmental noise in the dynamic signal in the experimental testing. The important thing to note here is, even though there is a considerable difference in numerical and experimental results for the optimized parametric values, there is a notable rise in the percentage increment of SampEn values with

optimized parametric values for the experimental results. This increment will definitely lead to higher crack identification sensitivity and be useful in crack identification process when the proposed method is employed in real world crack detection scenarios.

5.3 Summary

In this chapter, the crack identification sensitivity of the proposed breathing crack identification methodology for lower sinusoidal excitation frequencies are improved by parametric optimization of SampEn and WT. The numerical crack identification sensitivity for 45 rad/s excitation is improved by optimizing the parametric values of SampEn and WT in separate optimization loops. The parametric Optimization of SampEn improved the respective sensitivity from 22% to 16%, and WT optimization further pushed it to 8%. Then the numerical percentage increment value of SampEn at 25% crack depth is compared with the experimental values for the 25% crack beam. The experimental results showed an improvement due to parametric optimization which validates the parametric optimization process.

Both this and previous chapters covered the crack identification of the breathing crack cantilever beam under sinusoidal excitations. Moving forward in the dynamic complexity in the study presented in this thesis, the next chapter covers one important dynamic behavior experienced by almost all the structures: random vibration; and specifically breathing crack identification under random excitations using FRF as an add-in tool.

Chapter 6

Breathing Crack Identification under Random Excitations

Random excitation, perhaps the most common excitation type experienced by engineering structures, is studied in this chapter to evaluate the breathing crack identification using the proposed technique. In order to tackle the added complexity due to the dynamic nature of random signals itself, FRFs are now coupled with the entropy based crack identification technique. In this chapter, the results are obtained only using the experimental setup which is the arrangement for the applied case study, the breathing crack cantilever beam (illustrated in Section 3.1), which is now undergone random excitations during testing.

Section 6.1 explains the random excitation adapted crack identification technique, using FRF as an add-in tool with the existing method. The section covers a description of the overall technique, and the experimental setup used to obtain the results. Section 6.2 gives the experimental results of the breathing crack identification of the randomly excited case study beam, and the corresponding discussions.

6.1 The overall process of crack identification using entropy with WT and FRF as add-in tools

The proposed crack identification methodology using entropy with WT is straight forward in the case of a sinusoidal excitation of a cantilever beam with a breathing crack. But when it comes to random excitation, the crack identification methodology proposed for the sinusoidal excitations (in Section 4.1) is adapted to the situation with the help of FRF to tackle the complexity occurred due to the random vibration. This adapted methodology is illustrated in Figure 6.1.

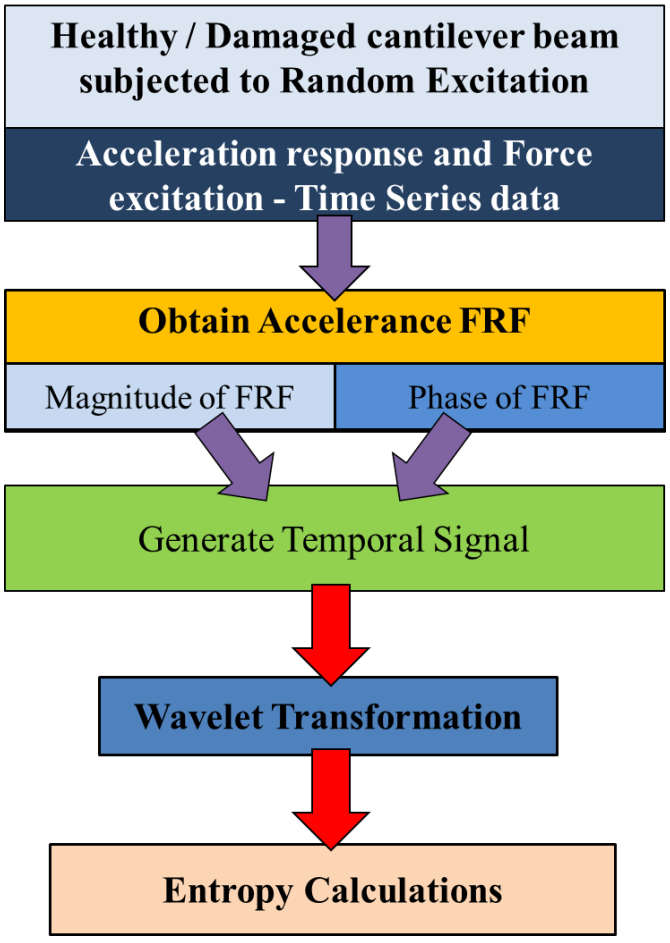

Figure 6. 1 - Flow chart of overall crack identification process of the random excitation adapted breathing crack identification technique.

As it is shown in Figure 6.1, the first step of the crack identification process is obtaining the time domain signals of the excitation and the response of the healthy and the damaged cantilever beam having a breathing crack. This is done by obtaining the force and the acceleration temporal signals from the experimental setup (refer Section 6.2) for the corresponding beams. Then, these signals are processed further and accelerance FRFs are calculated.

During this analysis, accelerance FRF is chosen over other FRF measures available, because the accelerations can be easily measured by readily available accelerometers. These experimentally measured FRFs have two components: magnitude and phase. These magnitude and phase values are used to re-generate a time domain signal, $w(t)$, following a method similar to inverse Fourier transformation. This is done using the following equation;

$$w(t) = a_0 + \sum_{i=1}^{N_f} a_i \sin(2\pi\ f_i\ t - \phi_i) \tag{6.1}$$

where, t is any time instance in the time domain, a_0 is the magnitude of the FRF signal at the zero frequency value (0 Hz) in the frequency-magnitude plot (refer Figure 6.4), N_f is the number of frequency increments in the frequency-magnitude plot, a and ϕ are FRF magnitudes, FRF phase values respectively at corresponding frequency values (f) of the corresponding frequency-magnitude and frequency-phase plots. Once this time domain signal is produced, it is now possible to follow the same crack identification procedure proposed in Section 4.1 using WT and entropy. The SampEn is calculated using 20,000 data samples in the generated time domain signal to achieve the converged results. Finally, the SampEn values at different crack

levels and healthy beam are calculated to find the percentage increment of SampEn at respective crack levels.

In the next section, the experimental setup is illustrated which is used to obtain the experimental results.

6.2 Experimental setup of the breathing crack cantilever beam under random excitation

The same cantilever beam experimental setup given in Section 4.2 is used with some minor changes to obtain both force and acceleration signals. Beams with both 25% and 50% crack depth percentages are selected for the experimental testing. The constructions of the beams are given in Section 4.2.

Figure 6.2 illustrates the experimental setup for obtaining the dynamic response from the 50% crack depth percentage beam. The beam is tightly clamped using four bolts to a steel clamping post which is solidly fixed to the concrete test bench. The free end of the beam is randomly excited using the shaker (The Modal Shop – model 2100E11). PCB Piezotronics model 352A24 accelerometer weighing 0.8 g (sensitivity is 10.2 mV/(m/s2) with ± 10% uncertainty) is located 0.20 m away from the free end of the beam. The force signal is measured using an integrated circuit piezoelectric (ICP) type force sensor from Piezotronics (model 208C01). The sensitivity of the force sensor is 112,410 mV/kN ($\pm$ 15%). The random signal generation and data acquisition are done using the same LMS SCADAS Mobile (type SCM05) data acquisition hardware which is integrated with the LMS Test.Lab software platform.

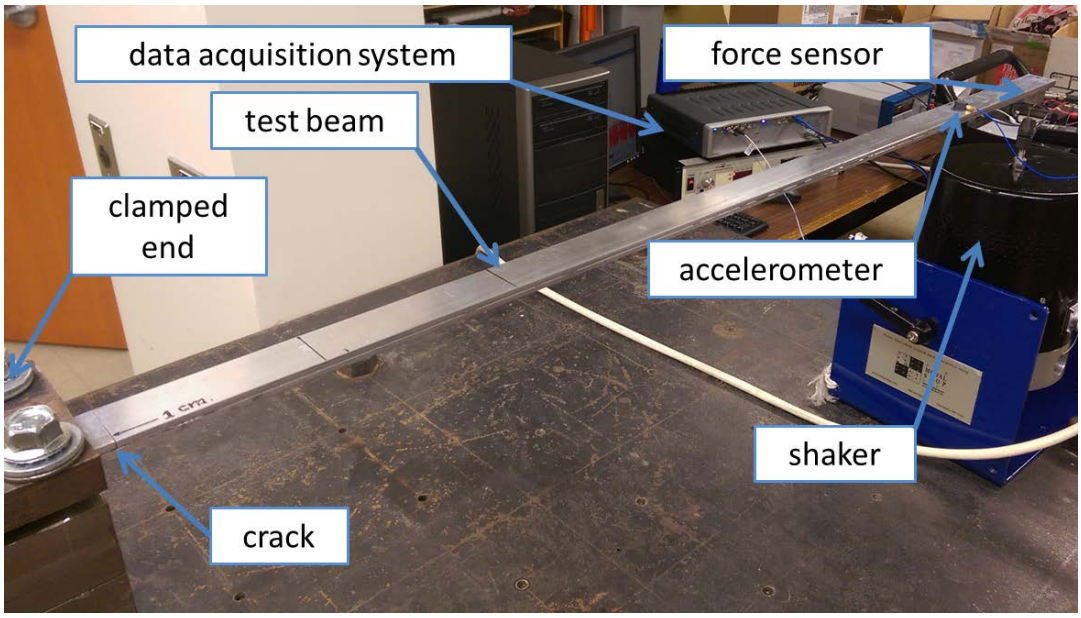

(a)

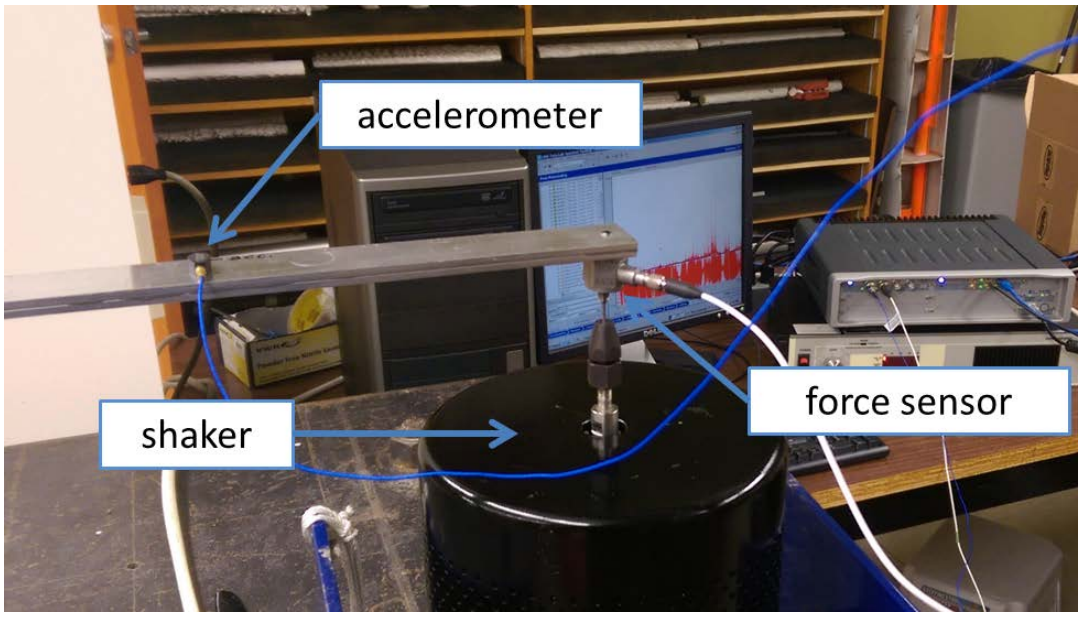

(b)

Figure 6. 2 - The experimental setup for obtaining excitation and responses of damaged and healthy aluminum alloy cantilever beams (a) the whole setup for testing of the beam with 50% crack depth percentage (b) the free end of the beam.

6.3 Results and discussions

This section presents the results and corresponding discussions pertaining to the experimental study of the crack identification of the cantilever beams; the experimental setup is described in the previous section and the crack identification method is elaborated in Section 6.1.

The three experimental aluminum alloy cantilever beams, i.e. healthy beam, 25% crack depth percentage beam and 50% crack depth percentage beam, are excited at the free end of those beams with a random excitation. This random excitation is a pure white noise ranging from 0 ~ 100 Hz is used for the random excitation. This excitation range covers the first and the second modal frequencies of the tested beams. Measurements include raw acceleration-time (response) and force-time (reference) data for the three beams. Figure 6.3 shows a snapshot (taken from the graphical user interface of the LMS Test.Lab software platform) of one of the reference (force-time measurements) data samples from the 50% crack depth percentage beam.

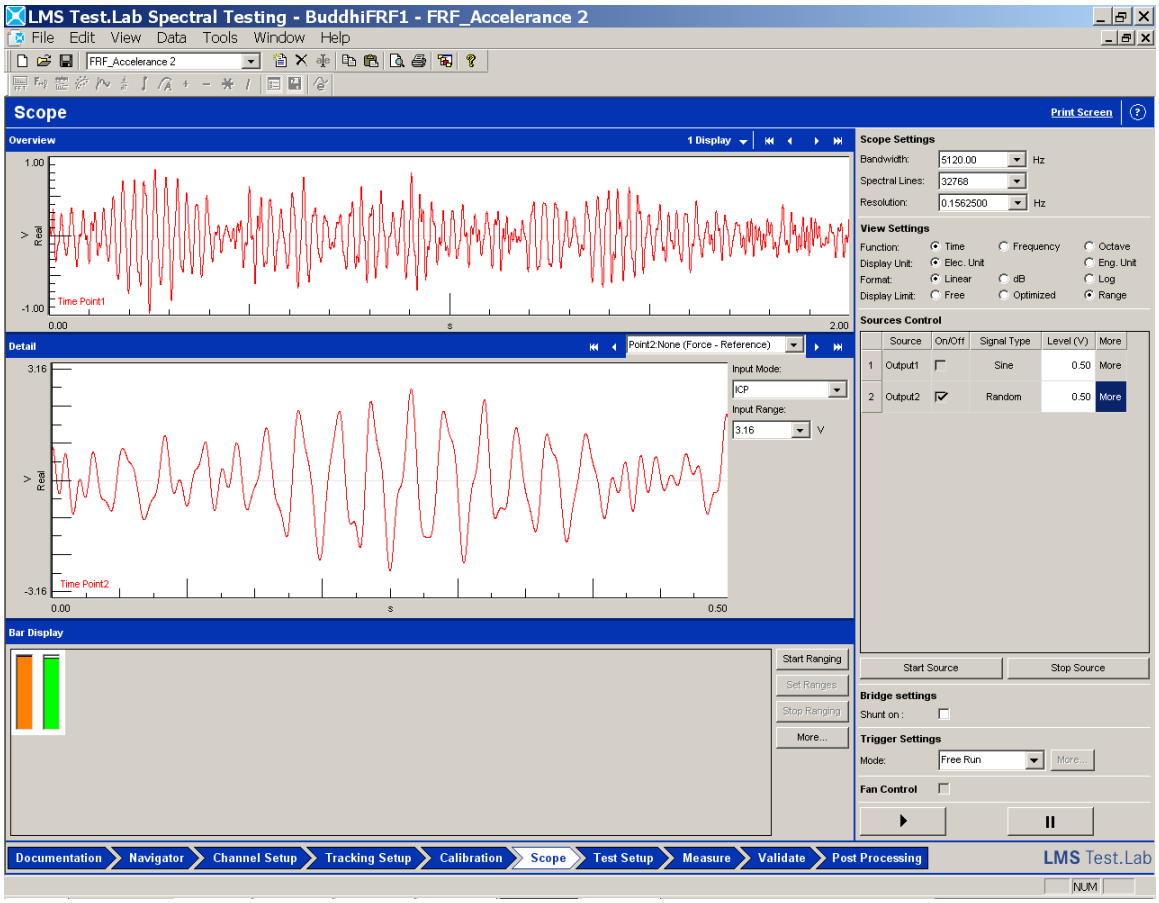

Figure 6. 3 - Graphical user interface snapshot of the force-time reference signal for the 50% crack depth percentage beam.

The time series data of force (reference) and acceleration (response) data are used by the LMS Test.Lab data analysis software platform to compute the accelerance FRFs. The Hanning window is applied to both reference and response data before calculating the FRFs to reduce the effect of spectral leakage. Corresponding FRFs are calculated for 10 consecutive runs, and linearly averaged to reduce the noise. In this experimental study, the FRF estimator H_v is used to compute the accelerance FRFs. Figure 6.4 illustrates one such FRFs generated for the 50% crack beam. The figure shows both amplitude (plot on the top) and phase (plot on the bottom) changes of the FRF with the frequency.

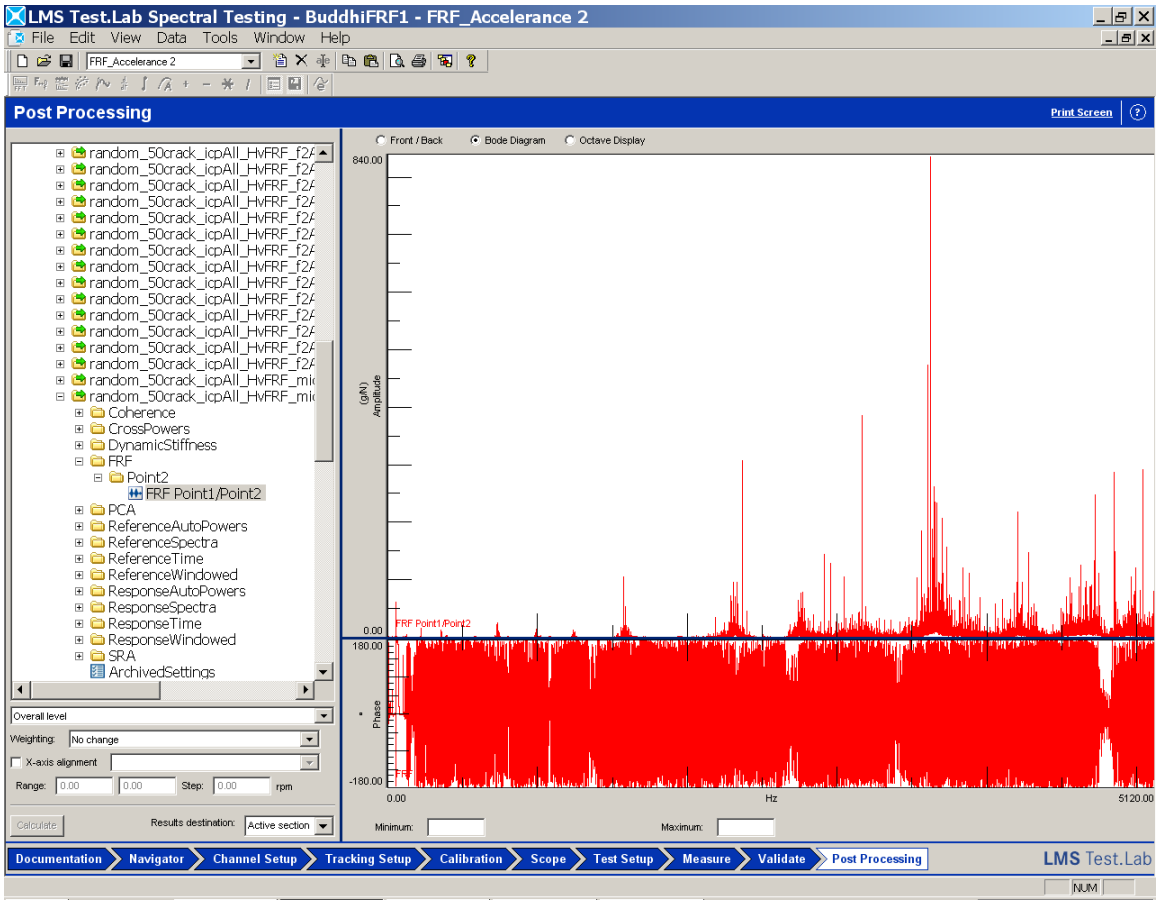

Figure 6. 4 - Graphical user interface snapshot of the accelerance FRF for the 50% crack depth percentage beam.

For each beam (i.e. healthy, 25% crack and 50% crack), the experiment is repeated for 10 runs. This is done to obtain an average value for the final SampEn values for each beam. The obtained FRF amplitudes and phase values are substituted in equation (6.1) and the corresponding temporal signals are generated for two seconds. It should be noted that the FRF amplitudes and phase values are selected from 0 Hz to 400 Hz of the frequency range. This is done to avoid the noisy FRF values obtained for the higher frequency ranges (< 400 Hz) possibly due to noise present in the output vibration signal, when the input dynamic force is accurately generated and measured with 0 - 100 Hz frequency. Then, 20,000 discrete data points are selected from these

generated temporal signals, and first these temporal signals are transformed to wavelet coefficient using WT. The same WT family of 'symlet2' is used in the calculations, which is readily available in the MatLab® WT package. The scale of the WT used is 240 and the WT is done for 9 consecutive times one WT after another WT manner. This is then followed by the SampEn calculations on the wavelet transformed data, and same number of data points of the wavelet coefficient (20,000 data points) is used in the entropy calculations. The parametric values of 'm' and 'r' for SampEn are 2 and 0.2 times SD of data respectively. Finally, the percentage increment of SampEn values for both 25% and 50% crack beams are calculated for all 10 runs each. These results are tabulated in Table 6.1.

Table 6. 1 - Percentage increment of SampEn for 25% and 50% crack beams for ten experimental runs.

	Sample Entropy values			***Percentage increment of SampEn compared to the healthy beam (%)***	
Run No.	Healthy beam	25% Crack beam	50% Crack beam	25% Crack beam	50% Crack beam
1	0.00109	0.00680	0.01252	365.1	756.3
2	0.00186	0.00914	0.01260	524.8	761.8
3	0.00143	0.00262	0.01162	79.0	694.5
4	0.00164	0.00932	0.01602	537.0	995.2
5	0.00142	0.00537	0.01411	266.8	864.9
6	0.00159	0.00821	0.01262	461.2	763.2
7	0.00151	0.00747	0.01530	410.9	946.0
8	0.00121	0.00803	0.01811	448.7	1138.2
9	0.00155	0.00910	0.01250	522.2	754.7
10	0.00132	0.00213	0.01530	45.7	946.2
AVG = 0.00146				**AVG = 366.1**	**AVG = 832.1**
				SD = 170.8	**SD = 133.7**

In Table 6.1, AVG is the average and SD is the standard deviation of the 10 runs. The second, third and the fourth columns give the SampEn of healthy, 25% crack and 50% crack beams respectively for each run. The average SampEn value of healthy beam is calculated as 0.00146 for the healthy beam. This value is used to calculate the percentage increment of SampEn values of cracked beams (which are with respect to the healthy beam) shown in the fifth and the sixth columns. The averaged percentage increment of SampEn for the 25% crack beam is 366.1%, on the other hand for 50% crack beam it is 832.1%. These averaged values show a clear increase in the percentage increment of SampEn values from 25% crack beam to the 50% crack beam. The SD values give confidence over the percentage increment of SampEn for both cracked beams. Smaller the SD values are, higher the confidence will be. From Table 6.1, these SD values are 170.8% and 133.7% for 25% crack beam and 50% crack beam respectively. If percentage fractions of the SD values are considered with respect to the corresponding AVG values, it is 46.7% for the 25% crack beam and 16.1% for the 50% crack beam. This is due to the fact that, larger crack depths produce significantly larger breathing effects compared to comparatively smaller crack depths. This leads to more consistent SampEn values for larger crack depths, and also for percentage increment of SampEn values. This leads to lower SD values for the larger crack depths, giving more confidence over identification of larger cracks using the proposed methodology.

6.4 Summary

This chapter covered the breathing crack identification of the applied case study under random excitation. The random excitation adapted crack identification methodology with FRF is given first, and then the randomly excited cantilever test beam setup details are given in the second

section. The experiment setup is used to observe the crack identification results for both 25% and 50% crack beams, and ten similar runs are conducted to have better understanding of the percentage increment of SampEn for different initiations of the test runs. The final section covers the results and discussions of these results and it is found that, there is a distinct difference between the averaged percentage increments of SampEn of 25% crack beam and the 50% crack beam. The SD values suggest higher confidence in breathing crack identification of the 50% crack beam compared to the 25% crack beam.

Chapter 7

Conclusions and Future Works

During the lifespan of a structure, it is subjected to various loading conditions including perhaps some abrupt loadings which are not even foreseen on the design board, and some absurd weather and operating conditions; and in addition, serving beyond their designed lifespan is not so rare for most of the today's structures. Due to these facts, engineering structures are always prone to structural damages; where modern engineering has to go beyond its limits exceeding designing and manufacturing boundaries, exploring efficient and effective damage detection techniques.

Breathing cracks are a special type of damage type evident in structures which experience dynamic loading conditions. During vibration of the cracked structure, the crack exhibits repetitive open-close breathing like phenomenon, hence the cracks are termed as breathing cracks. In the last few decades, vibration-based damage detection techniques have gained much interest among both the industrial and academic researches due to their versatile on-line damage detection capabilities. The same technique has evolved in to breathing crack identification, where it faces its own challenges.

Breathing phenomenon, the central feature of these cracks, generates crack severity related irregularities in the vibration response of the cracked structure. In this thesis, the concept of

entropy is employed to quantify these irregularities, ultimately relating these entropy values to the crack severities which caused these irregularities. WT, which is able to magnify perturbations, is employed with entropies to aid in the crack identification process, which leads to high sensitivity breathing crack identification results under certain conditions of the numerical computations. Then FRFs are combined with the crack identification method to tackle one important dynamic condition experienced by structures: random vibrations.

Breathing crack identification capabilities of the proposed methodology is studied numerically and experimentally, using a selected case study. A cantilever beam with a breathing crack is chosen as the case study due to experimental and numerical flexibility in both setting-up and testing/analyzing the system for different excitation conditions while exhibiting challenging grounds in its own. The iterative numerical model built for the applied case study is used to generate accurate vibrational responses, while acceleration measurements are measured from the experimental setup for the analysis.

All the in-house analysis codes written using the MatLab® R2015a software package has been published open-source project (refer Appendix E), which can be used by anyone, modify them as per their requirements, and perhaps further improve them for a better future for damage detection.

7.1 Viability and effectiveness of entropy in breathing crack identification

This thesis is basically divided in to three analytical sections, Chapters 4, 5 and 6 as they are named. Chapter 4 covers the crack identification under sinusoidal excitation, which provides

basic understanding of how the proposed method is employed in crack identification. Results of this chapter conclude some important findings listed as below.

1) The proposed breathing crack identification technique is capable of high sensitivity crack identification for small and initial crack depth of only 3% of the beam thickness with more than 200% increment in SampEn compared with the healthy beam. The experimental results are in good agreement with the numerical results and conclude the fact that larger crack depths generate more considerable breathing effect, leading to better identification grounds for them.
2) The computational time is significantly reduced with QASE by about 325 times at 20,000 data samples compared to SampEn.

Chapter 5 is dedicated to find a remedy for a problem identified in chapter 4. The breathing crack identification sensitivities for lower excitations are not as good as for the higher excitations. This is rectified up to some extent by optimizing the parametric values of SampEn and WT. The findings of this chapter conclude:

3) Using the parametric optimization, for sinusoidal excitations closer to the first modal frequency of the cantilever beam, 8% crack depth percentage can be identified which is much more sensitive compared with the case with non-optimized parametric values (22%).

In chapter 6, the proposed breathing crack identification technique is experimentally tested for more realistic excitation in real world, i.e. random excitation. This added complexity is handled with the help of FRFs. The experimental results conclude that:

4) There is a significant sample entropy percentage increment due to the breathing crack on the beam compared with the health beam. For the 25% crack beam, it is 366.1% of

sample entropy percentage increment in average for the ten experimental runs and for the 50% crack beam this particular value is 832.1%.

In addition to these conclusions, in overall, the advantages of the proposed breathing crack identification technique are:

1) The proposed technique requires only two sensors for breathing crack identification in the case of when it is required to handle the most complex type of vibration conditions under random excitations. Besides that, for simple sinusoidal vibrations, only one sensor is required.
2) The method can be used for damage identification under general structural dynamic working conditions where it does not demand any special condition on its excitations; for example, sinusoidal excitation can be of any frequency, and the crack identification under random excitations with no special requirement can be realized as well.
3) The method is also capable of on-line real-time continuous crack identification with the help of the high calculation efficient QASE measurement.
4) Furthermore, the proposed technique can also be applied to other types of complex structures, such as plates and shells with breathing cracks.

These advantages highlight the effectiveness of the proposed breathing crack identification technique as a practical and further developable damage identification methodology.

7.2 Future works

The proposed breathing crack identification technique will definitely benefit from further analysis. One key area is effective handling of noisy signals which would hugely increase the crack identification sensitivities of the proposed method. Especially for smaller crack depths, the breathing effect is masked by the noise presence in the vibration signals. This can be rectified by developing an effective filtering method, which will remove the noise effect while preserving the breathing effect. Another key area will be development of new entropy measures. Even though QASE is computationally fast, it cannot always give meaningful quantification of the breathing phenomenon. Therefore, a hybrid-type of entropy, which combines both good characteristics from SampEn and QASE, will be a better entropy measure to realize fast and accurate crack identification.

References

[1] Cheng SM, Swamidas A, Wu XJ, and Wallace W, 1999,“Vibrational response of a beam with a breathing crack,” Journal of Sound and Vibration, **225**(1), pp. 201–208.

[2] Semperlotti F., Wang K. W., and Smith E. C., 2009,“Localization of a breathing crack using nonlinear subharmonic response signals,” Appl. Phys. Lett., **95**(25), p. 254101.

[3] Leverick G., 2013,“Entropy Measures in Dynamical Systems and Their Viability in Characterizing Bipedal Walking Gait Dynamics,” Master's dissertation, Department of Mechanical Engineering, University of Manitoba, Manitoba.

[4] Chondros T. G., Dimarogonas A. D., and YAO J., 2001,“Vibration of a beam with a breathing crack,” Journal of Sound and Vibration, **239**(1), pp. 57–67.

[5] Yan G., De Stefano A., Matta E., and Feng R., 2013,“A novel approach to detecting breathing-fatigue cracks based on dynamic characteristics,” Journal of Sound and Vibration, **332**, pp. 407–422.

[6] Douka E., and Hadjileontiadis L. J., 2005,“Time–frequency analysis of the free vibration response of a beam with a breathing crack,” NDT & E International, **38**(1), pp. 3–10.

[7] Andreaus U., and Baragatti P., 2009,“Fatigue crack growth, free vibrations, and breathing crack detection of aluminium alloy and steel beams,” The Journal of Strain Analysis for Engineering Design, **44**(7), pp. 595–608.

[8] Kirmsher P. G., 1944,“The effect of discontinuities on the natural frequency of beams,” Proceedings of the American Society of Testing and Materials, pp. 897–904.

[9] Giannini O., Casini P., and Vestroni F., 2013,“Nonlinear harmonic identification of breathing cracks in beams,” Computers & Structures, **129**, pp. 166–177.

[10] Wu N., 2015,“Study of forced vibration response of a beam with a breathing crack using iteration method,” J Mech Sci Technol, **29**(7), pp. 2827–2835.

[11] Shannon C. E., 2001,“A mathematical theory of communication,” SIGMOBILE Mob. Comput. Commun. Rev., **5**(1), p. 3.

[12] Wang Q., and Deng X., 1999,“Damage detection with spatial wavelets,” International Journal of Solids and Structures, **36**(23), pp. 3443–3468.

[13] Wu N., and Wang Q., 2011,“Experimental studies on damage detection of beam structures with wavelet transform,” International Journal of Engineering Science, **49**(3), pp. 253–261.

[14] Ewins D. J., 2000. *Modal testing: Theory, practice, and application / D.J. Ewins,* 2nd ed., Research Studies Press, Baldock.

[15] Doebling S. W., Farrar C. R., Prime M. B., and Shevitz D. W., 1996,“Damage identification and health monitoring of structural and mechanical systems from changes in their vibration characteristics: A literature review,” Report for Los Alamos National Lab Report no. LA-13070-MS.

[16] Salawu O. S., 1997,“Detection of structural damage through changes in frequency: A review,” Engineering Structures, **19**(9), pp. 718–723.

[17] Doebling S. W., Farrar C. R., and Prime M. B., 1998,“A Summary Review of Vibration-Based Damage Identification Methods,” The Shock and Vibration Digest, **30**(2), pp. 91–105.

[18] Montalvao D., 2006,“A Review of Vibration-based Structural Health Monitoring with Special Emphasis on Composite Materials,” The Shock and Vibration Digest, **38**(4), pp. 295–324.

[19] Yan Y. J., Cheng L., Wu Z. Y., and Yam L. H., 2007,“Development in vibration-based structural damage detection technique,” Mechanical Systems and Signal Processing, **21**(5), pp. 2198–2211.

[20] Ismail F., Ibrahim A., and Martin H. R., 1990,“Identification of fatigue cracks from vibration testing,” Journal of Sound and Vibration, **140**(2), pp. 305–317.

[21] Lee Y.-S., and Chung M.-J., 2000,“A study on crack detection using eigenfrequency test data,” Computers & Structures, **77**(3), pp. 327–342.

[22] Rizos P. F., Aspragathos N., and Dimarogonas A. D., 1990,“Identification of crack location and magnitude in a cantilever beam from the vibration modes,” Journal of Sound and Vibration, **138**(3), pp. 381–388.

[23] Khoo L. M., Mantena P. R., and Jadhav P., 2004,“Structural Damage Assessment Using Vibration Modal Analysis,” Structural Health Monitoring, **3**(2), pp. 177–194.

[24] Owolabi G. M., Swamidas A. S. J., and Seshadri R., 2003,“Crack detection in beams using changes in frequencies and amplitudes of frequency response functions,” Journal of Sound and Vibration, **265**(1), pp. 1–22.

[25] Park N.-G., and Park Y.-s., 2005,“Identification of damage on a substructure with measured frequency response functions,” J Mech Sci Technol, **19**(10), pp. 1891–1901.

[26] Qu F., Zou D., and Wang X., 2004, Substructural Damage Detection Using Neural Networks and ICA, *Advances in Neural Networks – ISNN 2004*, Hutchison D., Kanade T., Kittler J., Kleinberg J. M., Mattern F., Mitchell J. C., Naor M., Nierstrasz O., Pandu Rangan

C., Steffen B., Sudan M., Terzopoulos D., Tygar D., Vardi M. Y., Weikum G., Yin F.-L., Wang J., and Guo C., eds., Springer Berlin Heidelberg, Berlin, Heidelberg, pp. 750–754.

[27] Su Z., and Ye L., 2004,“An intelligent signal processing and pattern recognition technique for defect identification using an active sensor network,” Smart Mater. Struct., **13**(4), pp. 957–969.

[28] Yuen K.-V., and Lam H.-F., 2006,“On the complexity of artificial neural networks for smart structures monitoring,” Engineering Structures, **28**(7), pp. 977–984.

[29] Chou J.-H., and Ghaboussi J., 2001,“Genetic algorithm in structural damage detection,” Computers & Structures, **79**(14), pp. 1335–1353.

[30] Moslem K., and Nafaspour R., 2002,“Structural damage detection by genetic algorithms,” AIAA journal, **40**(7), pp. 1395–1401.

[31] Mallat S. G., 1999. *A wavelet tour of signal processing*, 2nd ed., Academic, San Diego, Calif., London.

[32] Rajasekaran S., and Varghese S. P., 2005,“Damage detection in beams and plates using wavelet transforms,” Computers and Concrete, **2**(6), pp. 481–498.

[33] Chondros T. G., and Dimarogonas A. D., 1998,“Vibration of a Cracked Cantilever Beam,” J. Vib. Acoust., **120**(3), pp. 742–746.

[34] Nahvi H., and Jabbari M., 2005,“Crack detection in beams using experimental modal data and finite element model,” International Journal of Mechanical Sciences, **47**(10), pp. 1477–1497.

[35] Morassi A., 1993,“Crack-Induced Changes in Eigenparameters of Beam Structures,” J. Eng. Mech., **119**(9), pp. 1798–1803.

[36] Vestroni F., and Capecchi D., 1996,“Damage Evaluation in Cracked Vibrating Beams Using Experimental Frequencies and Finite Element Models,” Journal of Vibration and Control, **2**(1), pp. 69–86.

[37] Chati M., Rand R., and Mukherjee S., 1997,“Modal Analysis of a Cracked Beam,” Journal of Sound and Vibration, **207**(2), pp. 249–270.

[38] Matveev V. V., and Bovsunvsky A. P., 2002,“Vibration-based diagnostics of fatigue damage of beam-like structures,” Journal of Sound and Vibration, **249**(1), pp. 23–40.

[39] Abraham O. N. L., and Brandon J. A., 1995,“The Modelling of the Opening and Closure of a Crack,” J. Vib. Acoust., **117**(3A), pp. 370–377.

[40] Nguyen V. K., and Olatunbosun O., 2007,“A proposed method for fatigue crack detection and monitoring using the breathing crack phenomenon and wavelet analysis,” Journal of Mechanics of Materials and Structures, **2**(3), pp. 399–420.

[41] Kolmogorov A. N., 1958,“New metric invariant of transitive dynamical systems and endomorphisms of lebesgue spaces,” Doklady of Russian Academy of Sciences, **119(5)**, pp. 861–864.

[42] Kolmogorov A. N., 1959,“Entropy per unit time as a metric invariant of automorphism,” Doklady of Russian Academy of Sciences,, **124**, pp. 754–755.

[43] Sinai Y. G., 1959,“On the notion of entropy of a dynamical system,” Doklady of Russian Academy of Sciences, **124**, pp. 768–771.

[44] Diambra L., Figueiredo J. de, and Malta C. P., 1999,“Epileptic activity recognition in EEG recording,” Physica A: Statistical Mechanics and its Applications, **273**(3-4), pp. 495–505.

[45] Richman J. S., and Moorman J. R., 2000,“Physiological time-series analysis using approximate entropy and sample entropy,” American journal of physiology. Heart and circulatory physiology, **278**(6), p. 49.

[46] Leverick G., Szturm T., and Wu C. Q., 2014,“Using entropy measures to characterize human locomotion,” Journal of biomechanical engineering, **136**(12), p. 121002.

[47] Ducksbury P. G., 2000,“Target detection and intelligent image compression,” *AeroSense 2000*, SPIE, pp. 86–97.

[48] Ducksbury P. G., and Varga M. J., 2001,“Feature detection and fusion for intelligent compression,” *Aerospace/Defense Sensing, Simulation, and Controls*, SPIE, pp. 162–173.

[49] Pincus S., and Kalman R. E., 2004,“Irregularity, volatility, risk, and financial market time series,” Proceedings of the National Academy of Sciences of the United States of America, **101**(38), pp. 13709–13714.

[50] Yan R., and Gao R. X., 2007,“Approximate Entropy as a diagnostic tool for machine health monitoring,” Mechanical Systems and Signal Processing, **21**(2), pp. 824–839.

[51] Zhang L., Xiong G., Liu H., Zou H., and Guo W., 2010,“Bearing fault diagnosis using multi-scale entropy and adaptive neuro-fuzzy inference,” Expert Systems with Applications, **37**(8), pp. 6077–6085.

[52] Yan R., Liu Y., and Gao R. X., 2012,“Permutation entropy: A nonlinear statistical measure for status characterization of rotary machines,” Mechanical Systems and Signal Processing, **29**, pp. 474–484.

[53] Wu S. D., Wu P.-H., Wu C. W., Ding J. J., and Wang C.-C., 2012,“Bearing Fault Diagnosis Based on Multiscale Permutation Entropy and Support Vector Machine,” Entropy, **14**(12), pp. 1343–1356.

[54] Yang Z., Chen X., Jiang Y., and He Z., 2013,“Generalised local entropy analysis for crack detection in beam-like structures,” Nondestructive Testing and Evaluation, **29**(2), pp. 133–153.

[55] Ren W. X., and Sun Z. S., 2008,“Structural damage identification by using wavelet entropy,” Engineering Structures, **30**(10), pp. 2840–2849.

[56] Rosso O. A., Blanco S., Yordanova J., Kolev V., Figliola A., Schürmann M., and Başar E., 2001,“Wavelet entropy: A new tool for analysis of short duration brain electrical signals,” Journal of Neuroscience Methods, **105**(1), pp. 65–75.

[57] Browne M., Dorn M., Ouellette R., Christaller T., Shiry S., and Center C., 2002,“Wavelet entropy-based feature extraction for crack detection in sewer pipes,” *6th International Conference on Mechatronics Technology, Kitakyushu, Japan*.

[58] Luzzato E., 2003,“Approximate computation of non-linear effects in a vibrating cracked beam,” Journal of Sound and Vibration, **265**(4), pp. 745–763.

[59] Krawczuk M., and Ostachowicz W. M., 1995,“Modelling and vibration analysis of a cantilever composite beam with a transverse open crack,” Journal of Sound and Vibration, **183**(1), pp. 69–89.

[60] Leverick G., Wu C., and Szturm T., 2015,“Coarse quantization in calculations of entropy measures for experimental time series,” Nonlinear Dyn, **79**(1), pp. 93–100.

[61] Abbate A., DeCusatis C. M., and Das P. K., 2002. *Wavelets and subbands: Fundamentals and applications*, Birkhauser, Boston.

[62] Rocklin G. T., Crowley J., and Vold H., 1985,“A comparison of H1, H2, and Hv frequency response functions,” *Proceedings of the 3rd international Modal Analysis Conference*, pp. 272–278.

[63] Prime M. B., and Shevitz D. W., 1996,“Linear and nonlinear methods for detecting cracks in beams,” Proceedings pages, **1437**, p. 1443.

[64] Rao S. S., 2004. *Mechanical vibrations,* 4th ed., Pearson Prentice Hall, Upper Saddle River, N.J.

Appendix A

Derivation of Dynamic Beam Equation of an Euler-Bernoulli Laterally Vibrated Beam

Before deriving the dynamic equation, let us consider derivation of the Euler-Bernoulli relationship for bending moment of a slender cantilever beam.

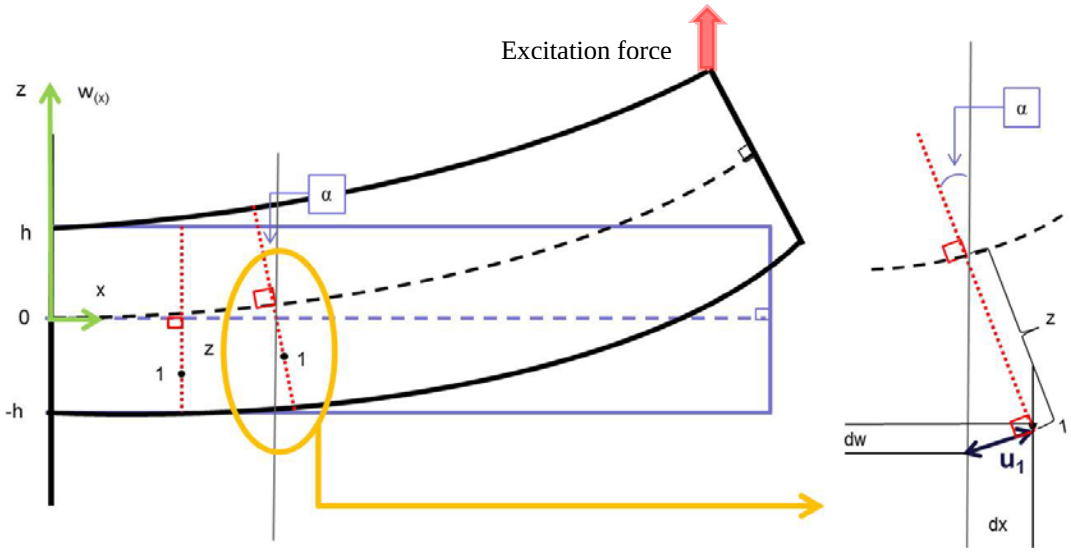

Figure A. 1 - Bending of a slender cantilever beam.

In Figure A.1, it illustrates bending of a slender cantilever beam. Let's consider a unit with of the beam (width of the beam is measured in the Y direction of the above figure).

A point (named as '1') is considered on an arbitrary cross section (illustrated in dotted lines) and then the deflection of the same point on the bent beam is considered to derive the bending moment relationship. This new position of point '1' is shown in a scaled-up (not to scale) format in the beside line diagram.

If the rotation of the considered cross section is a *small angle 'α'*,

From the line diagram it can obtain that, $\alpha \approx \tan\alpha = \frac{dw}{dx}$

If the point '1' is 'z' amount of distance from the line of bending, then;

Deflection of point 1, $$u_1 = z \tan\alpha = z \frac{dw}{dx} \quad \text{(A.1)}$$

Strain at point 1, $$\varepsilon_1 = \frac{du_1}{dx} = z \frac{d^2w}{dx^2} \quad \text{(A.2)}$$

If, the Young's modulus of the beam is taken as E, then using *Hooke's Law*, stress at a point;

$$\sigma = E\varepsilon \quad \text{(A.3)}$$

Therefore stress at point 1, $$\sigma_1 = E\,\varepsilon_1 = Ez \frac{d^2w}{dx^2} \quad \text{(A.4)}$$

Now, bending Moment, $$M = \int_{-h}^{h} \sigma_1 .\, z .\, dz \quad \text{(A.5)}$$

Now, taking the moment of inertia of the beam cross section about y-axis as 'I'

$$M = \int_{-h}^{h} Ez \frac{d^2w}{dx^2} .\, z .\, dz \quad \text{(A.6)}$$

$$M = E \frac{d^2w}{dx^2} \int_{-h}^{h} z \,.\, z .\, dz \quad \text{(A.7)}$$

$$M = E\frac{d^2w}{dx^2}\frac{h^3}{12} \tag{A.8}$$

Since width of the beam is 'one unit' then, $I = \frac{1.h^3}{12}$ (A.9)

Then, bending Moment is, $\boldsymbol{M = EI\ \frac{d^2w}{dx^2}}$ (A.10)

Now, as the next step, in order to derive the dynamic beam equation for the laterally vibrating beam, let's consider the free body diagram of the beam as shown in Figure A.2.

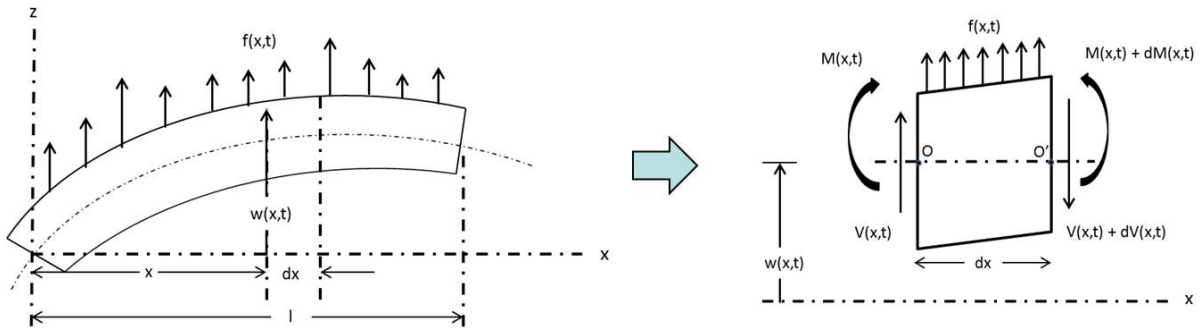

Figure A. 2 - Free body diagram of a slender beam under lateral vibration [64].

Before going to the derivations the variables used is presented below,

- V(x,t) - shear force
- M(x,t) - bending moment
- f(x,t) - external force per unit length of beam
- ρ - mass density of the beam
- A(x) - cross sectional area of the beam at distance x
- w - displacement of the beam in z direction
- t - time

Let's look at the derivation of the dynamic equation.

Inertia force acting on the element of the beam = $\rho A(x)\, dx \frac{\partial^2 w}{\partial t^2}(x,t)$ (A.11)

Then, equation of motion in the z-direction gives

$$-(V + dV) + f(x,t)dx + V = \rho A(x)\, dx \frac{\partial^2 w}{\partial t^2}(x,t) \quad \text{(A.12)}$$

The moment equation of motion about the y-axis passing through point O leads to,

$$(M + dM) - (V + dV)dx + f(x,t)dx\, \frac{dx}{2} - M = 0 \quad \text{(A.13)}$$

By writing, $dV = \frac{\partial v}{\partial x}dx \quad and \quad dM = \frac{\partial M}{\partial x}dx$

Then disregarding the terms involving second power in dx, equations (A.12) and (A.13) can be written as,

$$-\frac{\partial V}{\partial x}(x,t) + f(x,t) = \rho A(x)\, dx \frac{\partial^2 w}{\partial t^2}(x,t) \quad \text{(A.14)}$$

$$\frac{\partial M}{\partial x}(x,t) - V(x,t) = 0 \quad \text{(A.15)}$$

By using relation $V = \frac{\partial M}{\partial x}$ from equation (A.15) then equation (A.14) becomes,

$$-\frac{\partial^2 M}{\partial x^2}(x,t) + f(x,t) = \rho A(x)\, dx \frac{\partial^2 w}{\partial t^2}(x,t) \quad \text{(A.16)}$$

Then from equation (A.10),

$$M(x,t) = EI \frac{\partial^2 w}{\partial x^2}(x,t)$$

Substituting bending moment equation in equation (A.16), the dynamic equation for the laterally vibrating beam becomes,

$$\boldsymbol{EI}\frac{\boldsymbol{\partial^4 w}}{\boldsymbol{\partial x^4}}(\boldsymbol{x},\boldsymbol{t}) + \boldsymbol{\rho A}\frac{\boldsymbol{\partial^2 w}}{\boldsymbol{\partial t^2}}(\boldsymbol{x},\boldsymbol{t}) = \boldsymbol{f}(\boldsymbol{x},\boldsymbol{t}) \tag{A.17}$$

Appendix B

Derivation of Characteristic Function of a Laterally Vibrated Beam

At first, let us consider a single mode of vibration for the dynamic equation and for the free vibration of the beam,

Now for free vibration, $f(x,t) = 0$ in Figure A.2, and considering only one vibration mode, then equation (A.17) becomes;

$$EI\frac{\partial^4 w}{\partial x^4}(x,t) + \rho A\frac{\partial^2 w}{\partial t^2}(x,t) = 0 \tag{B.1}$$

The solution for this can achieved using 'variable separable' method,

$$w(x,t) = W_{(x)}T_{(t)} \tag{B.2}$$

Here, $W_{(x)}$ is the 'x' dependent part of the solution and $T_{(t)}$ is the 't (time)' dependent part of the solution. Substituting (B.2) in (B.1),

$$EI\frac{d^4 W_{(x)}}{dx^4}\,T_{(t)} + \rho A W_{(x)}\,\frac{d^2 T_{(t)}}{dt^2} = 0 \tag{B.3}$$

After dividing everything by $W_{(x)}T_{(t)}$ this can be re-written as,

$$EI\frac{d^4W_{(x)}}{dx^4}\frac{1}{W_{(x)}} + \rho A\frac{1}{T_{(t)}}\frac{d^2T_{(t)}}{dt^2} = 0 \quad \text{(B.4)}$$

After re-arranging, $$EI\frac{d^4W_{(x)}}{dx^4}\frac{1}{W_{(x)}} = -\rho A\frac{1}{T_{(t)}}\frac{d^2T_{(t)}}{dt^2} = constant \quad \text{(B.5)}$$

Then taking the constant as, $constant = \rho A\omega^2$

Now equation (B.5) becomes,

$$EI\frac{d^4W_{(x)}}{dx^4}\frac{1}{W_{(x)}} = -\rho A\frac{1}{T_{(t)}}\frac{d^2T_{(t)}}{dt^2} = \rho A\omega^2 \quad \text{(B.6)}$$

Now this equation can be separated into two parts, one with $W_{(x)}$ and another with $T_{(t)}$. These two equations are,

$$\frac{d^4W_{(x)}}{dx^4}\frac{1}{W_{(x)}} - \beta^4\omega^2 W_{(x)} = 0 \quad \text{(B.7)}$$

where, $\beta^4 = \frac{\rho A}{EI}\omega^2$

and $$\frac{d^2T_{(t)}}{dt^2} + \omega^2 T_{(t)} = 0 \quad \text{(B.8)}$$

Let's consider equation (B.7) because the equation with time function (i.e. equation (B.8)) is not an interest at this stage.

Assuming solution to the equation (B.7) as, $W_{(x)} = Ce^{sx}$

C and s are constants to be determined.

Then substituting back in equation (B.7) gives,

$$s^4 - (\beta)^4 = 0 \quad \text{(B.9)}$$

Then, $s_{1,2} = \pm \beta$ $s_{3,4} = \pm i\,\beta$

Then substituting back these in the assumed solution,

$$W_{(x)} = C_1 e^{s_1 x} + C_2 e^{s_2 x} + C_3 e^{s_3 x} + C_4 e^{s_4 x} \quad \text{(B.10)}$$

Equation (B.10) can also be expressed as;

$$W_{(x)} = C_1(cos\beta x + cosh\beta x) + C_2(cos\beta x - cosh\beta x) + C_3(sin\beta x + sinh\beta x) +$$

$$+ C_4(sin\beta x - sinh\beta x) \quad \text{(B.11)}$$

Then,

$$W_{(x)} = cos\beta x(C_1 + C_2) + sin\beta x(C_3 + C_4) + cosh\beta x(C_1 - C_2) + sinh\beta x(C_3 - C_4) \quad \text{(B.12)}$$

Taking, $(C_1 + C_2) = A_1$, $(C_3 + C_4) = A_2$, $(C_1 - C_2) = A_3$, $(C_3 - C_4) = A_4$

Now,

$$W(x) = A_1 cos\beta x + A_2 sin\beta x + A_3 cosh\beta x + A_4 sinh\beta x \quad \text{(B.13)}$$

Then for the nth mode of vibration, the Characteristic function of the beam becomes,

$$\boldsymbol{W_n(x) = A_1 cos\beta x + A_2 sin\beta x + A_3 cosh\beta x + A_4 sinh\beta x} \quad \text{(B.14)}$$

Where, $A_1, A_2, A_3 and\ A_4$ are new constants to be determined using boundary conditions.

Appendix C

Numerical Examples in Entropy Calculations

In this appendix, detailed calculation steps in calculating the two entropy measures used in this thesis, SampEn and QASE are given using a simple numerical example. Let's take a simple time domain data set as;

$$X(t) = \{0.825, 0.726, 0.538, 0.467, 0.825, 0.726, 0.538, 0.467\}$$

Now the number of data samples, $N = 8$ and let us take $m = 3$ and r = 0.1 for the entropy calculations.

C.1 Sample entropy calculation

Then according to equation (3.15) the template vectors are;

$$X(1) = \{0.825, 0.726, 0.538\}$$

$$X(2) = \{0.726, 0.538, 0.467\}$$

$$X(3) = \{0.538, 0.467, 0.825\}$$

$$X(4) = \{0.467, 0.825, 0.726\}$$

$$X(5) = \{0.825, 0.726, 0.538\}$$

$$X(6) = \{0.726, 0.538, 0.467\}$$

Then for $i = 1$ in equation (3.16), let's calculate the number of template vector matches using the Chebyshev distance;

$d\big[X_3(1),\ X_3(2)\big] = \max\big(\big|X_3(1)\ - X_3(2)\big|\big) = |0.726 - 0.538| = 0.188 > 0.1 \rightarrow$ Not a match

$d[X_3(1),\ X_3(3)] = \max(|X_3(1)\ - X_3(3)|) = |0.825 - 0.538| = 0.287 > 0.1$

$d[X_3(1),\ X_3(4)] = \max(|X_3(1)\ - X_3(4)|) = |0.825 - 0.467| = 0.358 > 0.1$

$d\big[X_3(1),\ X_3(5)\big] = \max\big(\big|X_3(1)\ - X_3(5)\big|\big) = |0.825 - 0.825| = 0.000 < 0.1 \rightarrow$ A match

$d[X_3(1),\ X_3(6)] = \max(|X_3(1)\ - X_3(6)|) = |0.726 - 0.538| = 0.188 > 0.1$

Then, recalling equation (3.16), the probabilistic values are,

$$B_1^3(0.1) = \frac{\#\ of\ j\ such\ that\ d[X_3(1),\ X_3(j)] \leq \mathrm{r}}{8-3-1} = \frac{1}{(8-3-1)} = \frac{1}{4}$$

Similarly,

$$B_2^3(0.1) = \frac{\#\ of\ j\ such\ that\ d[X_3(2),\ X_3(j)] \leq \mathrm{r}}{8-3-1} = \frac{1}{(8-3-1)} = \frac{1}{4}$$

$$B_3^3(0.1) = \frac{\#\ of\ j\ such\ that\ d[X_3(3),\ X_3(j)] \leq \mathrm{r}}{8-3-1} = \frac{0}{(8-3-1)} = 0$$

$$B_4^3(0.1) = \frac{\#\ of\ j\ such\ that\ d[X_3(4),\ X_3(j)] \leq \mathrm{r}}{8-3-1} = \frac{0}{(8-3-1)} = 0$$

$$B_5^3(0.1) = \frac{\#\ of\ j\ such\ that\ d[X_3(5),\ X_3(j)] \leq \mathrm{r}}{8-3-1} = \frac{0}{(8-3-1)} = 0$$

Then summing up all the above probabilistic values and we get,

$$B^3(0.1) = (N-m)^{-1} \sum_{i=1}^{N-m} B_i^m(r) = \frac{1}{5} * \frac{(1+1)}{4} = \frac{2}{5*4}$$

Now, for $m = 4$, similar calculations are done to obtain $A^4(0.1)$, which is found as;

$$A^4(0.1) = (N-m)^{-1} \sum_{i=1}^{N-m} A_i^{m+1}(r) = \frac{1}{4} * \frac{(1)}{3} = \frac{1}{4*3}$$

Then, sample entropy can be calculated as,

$$\boldsymbol{SampEn(3, 0.1, 8)} = -ln\left[\frac{A^4(0.1)}{B^3(0.1)}\right] = -ln\left[\frac{\frac{1}{4} * \frac{1}{3}}{\frac{1}{5} * \frac{2}{4}}\right] = \mathbf{0.18}$$

C.2 QASE calculation

At first it is necessary to calculate the quantized time series using equation (3.22). For QASE it is necessary use $2r$ value instead of r in calculating quantized time series [3]. In the chosen time series, $\min(X) = 0.467$ and then, the quantized time series is;

$$X_q = \{1, 1, 0, 0, 1, 1, 0, 0\}$$

Then the vector groups are created as follows for $m = 3$ condition.

$$X_q(1) = \{1, 1, 0\}$$

$$X_q(2) = \{1, 0, 0\}$$

$$X_q(3) = \{0, 0, 1\}$$

$$X_q(4) = \{0, 1, 1\}$$

$$X_q(5) = \{1, 1, 0\}$$

$$X_q(6) = \{1, 0, 0\}$$

Then vector identifiers are allocated for each vector group (recall equation (3.23)). According to equation (3.23), now $\lambda = 1$.

$$(\mathbf{1} \times \mathbf{1^0}) + (\mathbf{1} \times \mathbf{1^1}) + (\mathbf{0} \times \mathbf{1^2}) = \mathbf{2}$$

$$(\mathbf{1} \times \mathbf{1^0}) + (\mathbf{0} \times \mathbf{1^1}) + (\mathbf{0} \times \mathbf{1^2}) = \mathbf{1}$$

$$(\mathbf{0} \times \mathbf{1^0}) + (\mathbf{0} \times \mathbf{1^1}) + (\mathbf{1} \times \mathbf{1^2}) = \mathbf{1}$$

$$(\mathbf{0} \times \mathbf{1^0}) + (\mathbf{1} \times \mathbf{1^1}) + (\mathbf{1} \times \mathbf{1^2}) = \mathbf{2}$$

$$(\mathbf{1} \times \mathbf{1^0}) + (\mathbf{1} \times \mathbf{1^1}) + (\mathbf{0} \times \mathbf{1^2}) = \mathbf{2}$$

$$(\mathbf{1} \times \mathbf{1^0}) + (\mathbf{0} \times \mathbf{1^1}) + (\mathbf{0} \times \mathbf{1^2}) = \mathbf{1}$$

Now, let us create a matrixG_3, in which the first column gives the vector identifiers and the second column gives the number of occurrence if corresponding vector identifiers.

$$G_3 = \begin{bmatrix} 1 & 3 \\ 2 & 3 \end{bmatrix}$$

Similarly, the same matrix can be calculated for the case of $m = 3 + 1 = 4$. Let us call the corresponding matrix as G_4 and it is given below,

$$G_4 = [2 \quad 5]$$

Now using the occurrences of vector identifiers in G_3 and G_4 matrices it is possible to calculate $\hat{B}^m(2r)$ and $\hat{A}^{m+1}(2r)$ values (recall equations (3.25) and (3.26)).

$$\hat{B}^3(0.2) = (8-3)^{-1} \times \left\{\left(3 \times \frac{3-1}{8-3-1}\right) + \left(3 \times \frac{3-1}{8-3-1}\right)\right\} = \frac{3}{5}$$

$$\hat{A}^4(0.2) = (8-3)^{-1} \times \left(5 \times \frac{5-1}{8-3-1}\right) = 1$$

Then, QASE can be calculated as;

$$\boldsymbol{QASE(3, 0.2)} = -ln\left[\frac{\hat{A}^4(0.2)}{\hat{B}^3(0.2)}\right] = -ln\left[\frac{1}{\frac{3}{5}}\right] = \mathbf{-0.51}$$

Appendix D

Entropy Convergence Check

Figure D.1 shows the entropy convergence results. It is observed that, SampEn converges when the number of data samples are around 18,000. During the analysis 20,000 data samples are used in all the calculations.

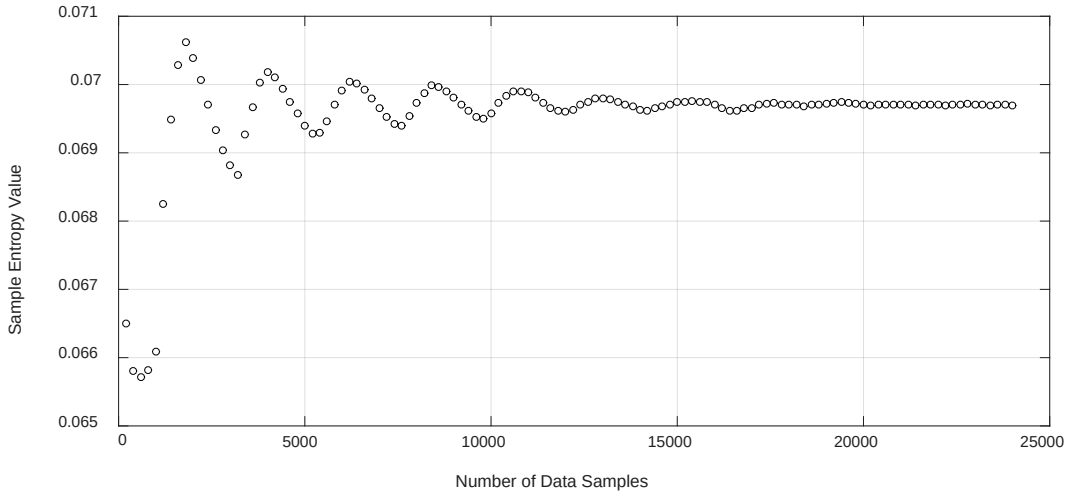

Figure D. 1 - Variation of sample entropy with different number of data samples showing the Entropy convergence.

Appendix E

The Outcome Research Materials

During the research, three research papers are completed. They are mentioned below chronologically;

1) Wimarshana B., Wu N., Wu C., 2016, “Application of entropy in identification of breathing cracks in a beam structure – simulation and experimental studies,” Journal of Structural Health Monitoring, (under review).

2) Wimarshana B., Wu N., Wu C., 2016, “Application of entropy in identification of breathing cracks in a beam structure – parametric study of sample entropy and wavelet transformation,” Journal of Structural Monitoring and Maintenance, (submitted).

3) Wimarshana B., Wu N., Wu C., 2016, “Identification of Breathing Cracks in a Beam Structure with Entropy,” In Proceedings of the SPIE, March 2016, Las Vegas, Vol. 9804, USA.

Then, in addition, all the MatLab® codes prepared for the proposed breathing crack identification technique have been published online as an open source project. The relevant codes can be found in the following Google drive link;

https://drive.google.com/folderview?id=0BzWbOFnPmyKwZUJ0MEVFblZFVTA&usp=sharing_eid&ts=577551c5